A Numerical Solution for the Barotropic Vorticity Equation Forced by an Equatorially Trapped Wave

by

James Christopher Ferguson
B.Sc., University of Victoria, 2004

A Thesis Submitted in Partial Fulfillment of the
Requirements for the Degree of

MASTER OF SCIENCE

in the Department of Mathematics and Statistics

A Numerical Solution for the Barotropic Vorticity Equation

Forced by an Equatorially Trapped Wave

by

James Christopher Ferguson
B.Sc., University of Victoria, 2004

Supervisory Committee

Dr. Boualem Khouider, Supervisor
(Department of Mathematics and Statistics)

Dr. Reinhard Illner, Departmental Member
(Department of Mathematics and Statistics)

Dr. Jane Ye, Departmental Member
(Department of Mathematics and Statistics)

Dr. William Merryfield, External Examiner
(Canadian Centre for Climate Modelling and Analysis)

Supervisory Committee

Dr. Boualem Khouider, Supervisor
(Department of Mathematics and Statistics)

Dr. Reinhard Illner, Departmental Member
(Department of Mathematics and Statistics)

Dr. Jane Ye, Departmental Member
(Department of Mathematics and Statistics)

Dr. William Merryfield, External Examiner
(Canadian Centre for Climate Modelling and Analysis)

Abstract

To understand the mechanisms of energy exchange between the tropics and the midlatitudes, it is necessary to develop simplified climate models. Motivated by linear wave theory, one such model is derived below. It captures the nonlinear interaction between barotropic and first baroclinic modes. In particular, it allows for the study of the barotropic response to a baroclinic forcing. Numerical methods for handling this nonlinear system are carefully developed and validated. The response generated by a physically realistic Kelvin wave forcing is studied and is found to consist mainly of one eastward propagating wave (phase-locked to the forcing) and two westward propagating (Rossby) waves. The Rossby waves are shown to be highly constrained by the initial parameters of the forcing and an explanation of this result is proposed.

Contents

List of Tables

List of Figures

Acknowledgements

I would like to thank my supervisor, Boualem Khouider, for the patience, guidance, and support he provided throughout this project. From him I have learned many things, not limited only to mathematics. For many engaging mathematical conversations, I would particularly like to thank Chris Garrett, Nick Henderson, Reinhard Illner, Brady Killough, Eric Kunze, Andrew MacRae, Mike Whittaker, and Jane Ye. Without the support and encouragement of Danielle Brown, Eric Dickstein, Janice Gaboury, Charlene Menezes, William Mohns, Adrian Neer, Machiko Oya, Tosha Tsang, and especially Angie Mallhi, I might not have made it to the end. Finally, I want to thank my brother Peter, who taught me more about life than he probably realizes.

James Ferguson

Chapter 1

Introduction

A topic of considerable interest to atmospheric scientists and meteorologists is the study of the interaction between water vapour and planetary scale dynamics in the tropics. Moist convection, in the form of organized deep convective super clusters, is a major heat source for tropical circulation and it has a significant impact on the prediction of weather and climate not only in the tropics but also in the mid-latitudes. Monsoons, the El Nino phenomenon, the tropical intraseasonal oscillation known as the Madden-Julian Oscillation (or MJO), and tropical storms are just a few other tropical phenomena that are also known to affect weather and climate in mid-latitudes in a major way. Hence, the need for a good understanding of the mechanisms of energy exchange between the Tropics and the mid-latitudes is obvious. Unfortunately, the General Circulation Models (or GCM's), which are used for weather and climate prediction, cannot adequately resolve many of these interactions on relevant temporal and spatial scales. This necessitates the development of simplified models that allow for detailed investigations of the effects of moisture on planetary wave dynamics as well as the interactions between tropical waves and the extra-tropics through the various teleconnection patterns.

It has been known for several decades that much of the variability in the tropics is a result of propagating (i.e. wave-like) disturbances which move parallel to the equator. Hence, we are interested in studying the effects of such waves on extra-tropical circulation. It has been pointed out in the literature, both from observations [21] and from theory [4, 8, 9, 10, 11, 12, 13], that convectively coupled tropical waves project heavily on the first baroclinic equatorial waves of Matsuno [17] but they propagate at a much slower speed than that of the dry case (50 ms^{-1} versus 15 ms^{-1}). Therefore, one approach is to consider only the dynamics of these dry waves without explicitly including moisture effects through the modification of the wave speed. Since much of the energy in the atmosphere is found in the vertically averaged (or barotropic) mode, a useful simplification for studying the lateral energy exchange (teleconnections) between the tropics and the mid-latitudes is to consider the interactions between the barotropic mode and equatorially trapped baroclinic waves. A recent model for such interactions uses a two mode model, representing the nonlinear interactions between the barotropic and the first baroclinic modes obtained by performing a Galerkin projection of the hydrostatic β-plane primitive equations [16]. We will use this model in our investigations.

The mathematical problems associated with modelling atmospheric phenomena are not trivial. Nonlinear coupled partial differential equations (PDE's) govern the flow of atmospheric waves and prohibit exact solutions in all but the most simplified cases. The development of numerical methods for prediction of the weather and climate is still very much an active field of research. This is especially true in the case of tropical climate modelling. Due to the risk of nonlinearities which may amplify without bound in finite time [19], the importance of choosing a numerical scheme with attractive conservation properties cannot be overemphasized.

A recent application of state-of-the-art methods from the applied mathematics community [14] to the problem of tropical climate modelling [8] showed that a non-oscillatory central scheme can accurately model equatorial waves without undue dissipation of energy. One particularly elegant feature of this scheme is in the way that shocks and steep gradients can be captured. However, atmospheric scientists use an alternative method for the same type of equations, developed by Arakawa to solve the incompressible barotropic vorticity equation [1]. The Arakawa Jacobian has obvious merits, most notably the conservation of mean wave-number energy, thereby eliminating nonlinear instabilities.

In this thesis, we will study the nonlinear interaction of barotropic and baroclinic waves using numerical methods developed for the two mode tropical model mentioned above. The plan for the thesis is as follows. First, we present a model of the tropical atmosphere based on the primitive equations used in GCM's. We review the theory of the associated linear system and present a simplified tropical climate model using Galerkin projection methods. Next we study the numerical methods needed for the solution of the nonlinear system. The Arakawa Jacobian is studied, as well as the numerical solution of Poisson's equation, used to enforce the incompressibility constraint. These two chapters are a review of existing theory. Next, we validate the numerical methods. The main contribution of this work is an examination of the response generated by the barotropic flow when forced by an equatorially trapped Kelvin wave, which is relevant for understanding the impact of tropical convection and convectively coupled waves on weather and climate in the mid-latitudes.

Chapter 2

Mathematical Model

We begin with the hydrostatic Boussinesq equations using the equatorial β-plane approximation [15]:

$$\frac{D\mathbf{V}}{Dt} + \beta y \mathbf{V}^{\perp} + \nabla P = \mathcal{S}_{\nu} \tag{2.1}$$

$$\nabla \cdot \mathbf{V} + \frac{\partial W}{\partial z} = 0 \tag{2.2}$$

$$\frac{D\Theta}{Dt} + \frac{N^2 \theta_0}{g} W = \mathcal{S}_{\Theta} \tag{2.3}$$

$$\frac{\partial P}{\partial z} = g \frac{\Theta}{\theta_0} \tag{2.4}$$

Here $\mathbf{V}(x, y, z, t) = (U(x, y, z, t), V(x, y, z, t))$ is the horizontal velocity field, $W = W(x, y, z, t)$ is the vertical velocity, β is the gradient of the Coriolis force at the equator, $P = P(x, y, z, t)$ is the pressure, N is the buoyancy frequency (taken here to be a constant equal to 0.01 s^{-1}, $g = 9.80$ m s^{-2} is the gravitational acceleration, $\Theta = \Theta(x, y, z, t)$ is the potential temperature, $\theta_0 = 300$ K is a reference (constant background) potential temperature. The pressure gradient is the vector $\nabla P = \left(\frac{\partial P}{\partial x}, \frac{\partial P}{\partial y}\right)$ and the divergence of $\mathbf{V}$ is defined as $\nabla \cdot \mathbf{V} = \frac{\partial U}{\partial x} + \frac{\partial V}{\partial y}$.

The material derivative is defined by

$$\frac{D}{Dt} \equiv \frac{\partial}{\partial t} + U\frac{\partial}{\partial x} + V\frac{\partial}{\partial y} + W\frac{\partial}{\partial z} \tag{2.5}$$

and $\mathbf{V}^{\perp} = (-V, U)$. Sources and sinks of momentum and heat, respectively, are represented by $\mathcal{S}_\nu = \mathcal{S}_\nu(x, y, z, t)$ and $\mathcal{S}_\Theta = \mathcal{S}_\Theta(x, y, z, t)$. Using the rigid lid boundary conditions at $z = 0, H_T$ (where H_T is the height of the tropopause) implies that $W(z = 0) = W(z = H_T) = 0$.

These equations describe the approximate global atmospheric flow given certain approximations. The β-plane approximation is a linear approximation of the Coriolis parameter which, in the tropics, has a maximum error of around 14% [5]. The hydrostatic approximation assumes that the pressure at any point in the atmosphere is due to the weight of the air above it and is a reasonable approximation when vertical accelerations are small compared to the gravitational acceleration. The Boussinesq approximation assumes that variations in density are small enough to be neglected except when buoyancy is considered. The derivation of (2.1)-(2.4) from the Navier-Stokes equations can be found in a number of texts [5, 15, 18].

2.1 Linear Theory of Equatorially Trapped Waves

Before we tackle the more difficult problem associated with this nonlinear system, we shall investigate solutions to the linear system (found by linearizing about a rest state, or equivalently, by eliminating all products of prognostic variables). This theory is well known and is studied in many papers [17] and texts [5, 15, 18]. Our approach follows closely the exposition found in Majda's book [15]. We shall omit the sources and sinks of momentum for simplicity and decompose the remaining variables into a vertically averaged (so-called barotropic) component,

which we will denote using an overbar, and a baroclinic (i.e. varying with height) component expanded in vertical modes, as follows:

$$\begin{pmatrix} \mathbf{V} \\ P \end{pmatrix}(x,y,z,t) = \begin{pmatrix} \overline{\mathbf{v}} \\ \overline{p} \end{pmatrix}(x,y,t) + \sum_{n=1}^{\infty} \begin{pmatrix} \mathbf{v}^n \\ p^n \end{pmatrix}(x,y,t)\ G_n(z) \tag{2.6}$$

$$\begin{pmatrix} W \\ \Theta \\ \mathcal{S}_\Theta \end{pmatrix}(x,y,z,t) = \sum_{n=1}^{\infty} \begin{pmatrix} w^n \\ \theta^n \\ \mathcal{S}^n \end{pmatrix}(x,y,t)\ \frac{dG_n(z)}{dz}, \tag{2.7}$$

where the $G_n(z)$'s are as yet undetermined functions of z. Notice that due to the rigid lid boundary conditions and the equation for hydrostatic balance (2.4), the barotropic components of W and Θ vanish. Ignoring the barotropic components and considering only the baroclinic components for the moment, we may plug equations (2.6)-(2.7) into the linearized version of (2.1)-(2.4) to obtain:

$$\frac{\partial \mathbf{v}^n}{\partial t} + \beta y \mathbf{v}^n + \nabla p^n = 0 \tag{2.8}$$

$$\nabla \cdot \mathbf{v}^n G_n(z) + w^n \frac{d^2 G_n(z)}{dz^2} = 0 \tag{2.9}$$

$$\frac{\partial \theta^n}{\partial t} + \frac{N^2 \theta_0}{g} w^n = \mathcal{S}^n \tag{2.10}$$

$$\frac{g}{\theta_0}\theta^n = p^n \tag{2.11}$$

Combining (2.10) and (2.11) results in

$$w^n = \frac{g}{N^2\theta_0}\left(\mathcal{S}^n - \frac{\theta_0}{g}\frac{\partial p^n}{\partial t}\right) \tag{2.12}$$

and substituting in (2.9) gives

$$\nabla \cdot \mathbf{v}^n G_n(z) + \frac{g}{N^2\theta_0}\left(\mathcal{S}^n - \frac{\theta_0}{g}\frac{\partial p^n}{\partial t}\right)\frac{d^2 G_n(z)}{\partial z^2} = 0. \tag{2.13}$$

This is a Sturm-Liouville problem [7] and separable solutions exist for (2.13) if and only if

$$\frac{d^2 G_n(z)}{dz^2} = -\lambda_n^2 G_n(z). \tag{2.14}$$

Using the boundary conditions gives

$$\frac{dG_n(z)}{dz} = 0, \text{ at } z = 0, H_T, \quad \text{for } n = 1, 2, \ldots, \tag{2.15}$$

which implies that

$$G_n(z) = \cos(\lambda_n z), \quad \lambda_n = \frac{n\pi}{H_T}. \tag{2.16}$$

The separation of variables allows us to focus on the horizontal structure of the system, since each vertical mode (associated with the separation constant λ_n) will have a qualitatively similar structure. Accordingly, we will now study just the horizontal structure and we will make a few simplifications. For simplicity, we nondimensionalize by introducing a temperature scale 15 K $\approx \frac{H_T N^2 \theta_0}{\pi g}$, define a characteristic speed for each vertical mode, given by $c_n = N/\lambda_n$, and rescale the pressure by setting $p = p_n/c_n$, and omit the subscript n from the variables.

Combining (2.8), (2.13), and (2.14) gives

$$\frac{\partial u}{\partial t} - \beta y v + c_n \frac{\partial p}{\partial x} = 0 \tag{2.17}$$

$$\frac{\partial v}{\partial t} + \beta y u + c_n \frac{\partial p}{\partial y} = 0 \tag{2.18}$$

$$\frac{\partial p}{\partial t} + c_n \frac{\partial u}{\partial x} + c_n \frac{\partial v}{\partial y} = \mathcal{S}^n. \tag{2.19}$$

As in [18], it is useful to take $\frac{\partial}{\partial x}(2.18) - \frac{\partial}{\partial y}(2.17)$ gives

$$\frac{\partial^2 v}{\partial x \partial t} - \frac{\partial^2 u}{\partial y \partial t} + \beta y \left(\frac{\partial u}{\partial x} + \frac{\partial v}{\partial y} \right) + \beta v = 0. \tag{2.20}$$

It is worth noting that by eliminating the variables u and p, we may obtain an equation for v and $\mathcal{S}^n$ only, in the following way:

$$-\frac{\beta y}{c_n}\frac{\partial}{\partial t}(17) + \frac{1}{c_n^2}\frac{\partial^2}{\partial t^2}(18) - \frac{1}{c_n}\frac{\partial^2}{\partial y \partial t}(19) + \frac{\beta y}{c_n}\frac{\partial}{\partial x}(19) - \frac{\partial}{\partial x}(20), \tag{2.21}$$

which leads to

$$\frac{\partial}{\partial t}\left(\frac{\beta^2 y^2}{c_n^2} v + \frac{1}{c_n^2}\frac{\partial^2 v}{\partial t^2} - \triangle v \right) - \beta \frac{\partial v}{\partial x} = -\frac{1}{c_n}\frac{\partial^2 \mathcal{S}^n}{\partial y \partial t} + \frac{\beta y}{c_n}\frac{\partial \mathcal{S}^n}{\partial x}, \tag{2.22}$$

where $\triangle = \frac{\partial^2}{\partial x^2} + \frac{\partial^2}{\partial y^2}$. Introducing the Riemann invariant variables

$$q = \frac{1}{\sqrt{2}}(p+u) \quad \text{and} \quad r = \frac{1}{\sqrt{2}}(p-u),$$

we can rewrite (2.17)-(2.19) as

$$\frac{\partial q}{\partial t} + c_n \frac{\partial q}{\partial x} + c_n \left(\frac{\partial v}{\partial y} - \frac{\beta}{c_n} yv \right) = \frac{1}{\sqrt{2}c_n} \mathcal{S}^n \tag{2.23}$$

$$\frac{\partial r}{\partial t} - c_n \frac{\partial r}{\partial x} + c_n \left(\frac{\partial v}{\partial y} + \frac{\beta}{c_n} yv \right) = \frac{1}{\sqrt{2}c_n} \mathcal{S}^n \tag{2.24}$$

$$\frac{\partial v}{\partial t} + \frac{c_n}{\sqrt{2}} \left(\frac{\partial q}{\partial y} + \frac{\beta}{c_n} yq \right) + \frac{c_n}{\sqrt{2}} \left(\frac{\partial r}{\partial y} - \frac{\beta}{c_n} yq \right) = 0. \tag{2.25}$$

Before we exhibit the complete solution of this system, we will look at two special cases. First, consider when $v \equiv 0$ and $S^n \equiv 0$. This results in the simpler system

$$\frac{\partial q}{\partial t} + c_n \frac{\partial q}{\partial x} = 0 \tag{2.26}$$

$$\frac{\partial r}{\partial t} - c_n \frac{\partial r}{\partial x} = 0 \tag{2.27}$$

$$\frac{c_n}{\sqrt{2}} \left(\frac{\partial q}{\partial y} + \frac{\beta}{c_n} yq \right) + \frac{c_n}{\sqrt{2}} \left(\frac{\partial r}{\partial y} - \frac{\beta}{c_n} yq \right) = 0. \tag{2.28}$$

One simple exact solution for (2.26)-(2.28) is obtained by separation of variables assuming a zonally propagating wave solution. We rewrite $q(x,y,t) = \tilde{q}(x - c_n t)\alpha(y),\ r \equiv 0$, and substitute into (2.28) to give

$$\frac{\partial \alpha}{\partial y} + \frac{\beta}{c_n} y\alpha = 0, \tag{2.29}$$

which has a solution

$$\alpha = \alpha_0 e^{-\beta y^2/2c_n}.$$

This represents a wave travelling eastward and decaying as $y \to \pm\infty$. Similarly, we rewrite $r(x,y,t) = \tilde{r}(x + c_n t)\alpha(y),\ q \equiv 0$, and substitute into (2.28) to give

$$\frac{\partial \alpha}{\partial y} - \frac{\beta}{c_n} y\alpha = 0, \tag{2.30}$$

which has a solution

$$\alpha = \alpha_0 e^{\beta y^2/2c_n}.$$

This represents a wave travelling westward, but the solution is unphysical since for large $|y|$, $\alpha \to \infty$. Hence, only the eastward moving wave, called a Kelvin wave, is retained. Moreover, the equator acts as a waveguide, trapping this type of wave, since the wave decays in strength as it moves away from the equator. The quantity $\sqrt{c_n/2\beta}$, called the radius of deformation, measures the rate of decay of the wave with respect to its distance from the equator.

As a more general procedure, consider (2.22) in the absence of any forcing (i.e. $\mathcal{S}^n \equiv 0$) and look for plane wave solutions propagating zonally around the equator of the form

$$v(x, y, t) = Re\left\{v(y)e^{i(kx-\omega t)}\right\}. \tag{2.31}$$

Here, k is the wavenumber and ω is the frequency. The propagation speed of the wave is given by the phase speed ω/k and the group velocity, which is the velocity of a wave packet, is $c_g = \frac{d\omega(k)}{dk}$ [18]. Plugging this into homogeneous form of (2.22) gives

$$\frac{\partial^2 v}{\partial y^2} + \left(\frac{\omega^2}{c_n^2} - k^2 - \frac{k\beta}{\omega} - \frac{\beta^2 y^2}{c_n^2}\right) v = 0, \tag{2.32}$$

which is the equation of the harmonic oscillator of quantum mechanics. The solutions of this equation are well known and can be constructed using parabolic cylinder functions. As in the case of the Kelvin wave above, these solutions vanish as $y \to \pm\infty$, as is required.

We now return to our system (2.26)-(2.28), armed with the knowledge that we should look for solutions which decay exponentially in y and which are represented using parabolic cylinder functions. Hence, we introduce the parabolic cylinder functions given by

$$D_m(\eta) = 2^{-m/2} H_m(\eta/\sqrt{2}) e^{-\eta^2/4}, \tag{2.33}$$

where the H_m's are the Hermite polynomials defined by

$$H_m(\xi) = (-1)^m e^{\xi^2} \frac{\partial^m e^{-\xi^2}}{\partial \xi^m}, \ m \geq 0. \tag{2.34}$$

The variables may now be expanded in terms of the orthonormal basis

$$\phi_m^n(y) = \left(m!\sqrt{\pi c_n/\beta}\right)^{-1/2} D_m\left((2\beta/c_n)^{1/2} y\right), \tag{2.35}$$

in $L^2(\mathbb{R})$ with inner product $\langle f, g\rangle = \int f(\alpha)g(\alpha)d\alpha$. Here $\left(m!\sqrt{\pi c_n/\beta}\right)^{-1/2}$ is the normalization constant. We introduce the ladder operators of quantum mechanics given by

$$L_\pm^n = \frac{d}{dy} \pm \frac{\beta}{c_n} y \tag{2.36}$$

and the useful identities

$$L_-^n \phi_m^n(y) = -(2\beta/c_n)^{1/2}(m+1)^{1/2}\phi_{m+1}^n(y) \tag{2.37}$$

$$L_+^n \phi_m^n(y) = (2\beta/c_n)^{1/2}(m)^{1/2}\phi_{m-1}^n(y). \tag{2.38}$$

Expanding the variables in terms of the orthonormal basis in y

$$\begin{pmatrix} q \\ r \\ v \\ \mathcal{S}^n \end{pmatrix}(x,y,t) = \sum_{m=0}^{\infty} \begin{pmatrix} \tilde{q}_m \\ \tilde{r}_m \\ \tilde{v}_m \\ \tilde{\mathcal{S}}_m^n \end{pmatrix}(x,t)\phi_m^n(y) \tag{2.39}$$

and using the ladder operators and identities allows us to go from this formulation

$$\frac{\partial q}{\partial t} + c_n \frac{\partial q}{\partial x} + c_n L_-^n v = \frac{1}{\sqrt{2}c_n}\mathcal{S}^n \tag{2.40}$$

$$\frac{\partial r}{\partial t} - c_n \frac{\partial r}{\partial x} + c_n L_+^n v = \frac{1}{\sqrt{2}c_n}\mathcal{S}^n \tag{2.41}$$

$$\frac{\partial v}{\partial t} + \frac{c_n}{\sqrt{2}} L_+^n q + \frac{c_n}{\sqrt{2}} L_-^n r = 0 \tag{2.42}$$

to a formulation which involves explicit relationships between the coefficients of the basis expansion:

$$\frac{\partial \tilde{q}_m}{\partial t}\phi_m^n + c_n \frac{\partial \tilde{q}_m}{\partial x}\phi_m^n - \frac{c_n}{\sqrt{2}}(2\beta/c_n)^{1/2}(m+1)^{1/2}\tilde{v}_m\phi_{m+1}^n = \frac{1}{\sqrt{2}c_n}\tilde{\mathcal{S}}_m^n\phi_m^n \tag{2.43}$$

$$\frac{\partial \tilde{r}_m}{\partial t}\phi_m^n + c_n\frac{\partial \tilde{r}_m}{\partial x}\phi_m^n + \frac{c_n}{\sqrt{2}}(2\beta/c_n)^{1/2}(m)^{1/2}\tilde{v}_m\phi_{m-1}^n = \frac{1}{\sqrt{2}c_n}\tilde{\mathcal{S}}_m^n\phi_m^n \tag{2.44}$$

$$\frac{\partial \tilde{v}_m}{\partial t}\phi_m^n + \frac{c_n}{\sqrt{2}}(2\beta/c_n)^{1/2}(m)^{1/2}\tilde{q}_m\phi_{m-1}^n - \frac{c_n}{\sqrt{2}}(2\beta/c_n)^{1/2}(m+1)^{1/2}\tilde{r}_m\phi_{m+1}^n = 0. \tag{2.45}$$

Here, we have followed the Einstein summation convention, where repeated indices in a given term m are summed, e.g. $\tilde{v}_m\phi_m^n = \sum_{m=0}^{\infty}\tilde{v}_m\phi_m^n$. Since this summation is term by term independent, we can conveniently rewrite the system to allow direct comparison of basis coefficients in the following way:

$$\frac{\partial \tilde{q}_m}{\partial t}\phi_m^n + c_n\frac{\partial \tilde{q}_m}{\partial x}\phi_m^n - \frac{c_n}{\sqrt{2}}(2\beta/c_n)^{1/2}(m)^{1/2}\tilde{v}_{m-1}\phi_m^n = \frac{1}{\sqrt{2}c_n}\tilde{\mathcal{S}}_m^n\phi_m^n \tag{2.46}$$

$$\frac{\partial \tilde{r}_m}{\partial t}\phi_m^n + c_n\frac{\partial \tilde{r}_m}{\partial x}\phi_m^n + \frac{c_n}{\sqrt{2}}(2\beta/c_n)^{1/2}(m+1)^{1/2}\tilde{v}_{m+1}\phi_m^n = \frac{1}{\sqrt{2}c_n}\tilde{\mathcal{S}}_m^n\phi_m^n \tag{2.47}$$

$$\frac{\partial \tilde{v}_m}{\partial t}\phi_m^n + \frac{c_n}{\sqrt{2}}(2\beta/c_n)^{1/2}(m+1)^{1/2}\tilde{q}_{m+1}\phi_m^n - \frac{c_n}{\sqrt{2}}(2\beta/c_n)^{1/2}(m)^{1/2}\tilde{r}_{m-1}\phi_m^n = 0. \tag{2.48}$$

Since coefficients with negative index vanish, the first equation gives a single PDE for $\tilde{q}_0$ given by

$$\frac{\partial \tilde{q}_0}{\partial t} + c_n\frac{\partial \tilde{q}_0}{\partial x} = \frac{1}{\sqrt{2}c_n}\tilde{\mathcal{S}}_0^n(x,t), \tag{2.49}$$

and when combined with the third equation, a system coupling $\tilde{v}_0$ and $\tilde{q}_1$:

$$\frac{\partial \tilde{v}_0}{\partial t} + (\beta c_n)^{1/2}\tilde{q}_1 = 0 \tag{2.50}$$

$$\frac{\partial \tilde{q}_1}{\partial t} + c_n\frac{\partial \tilde{q}_1}{\partial x} - (\beta c_n)^{1/2}\tilde{v}_0 = \frac{1}{\sqrt{2}c_n}\tilde{\mathcal{S}}_1^n(x,t). \tag{2.51}$$

Higher order coefficients are related by the 3×3 system given by (for $m \geq 2$):

$$\frac{\partial \tilde{q}_m}{\partial t} + c_n\frac{\partial \tilde{q}_m}{\partial x} - (m\beta c_n)^{1/2}\tilde{v}_{m-1} = \frac{1}{\sqrt{2}c_n}\tilde{\mathcal{S}}_m^n(x,t) \tag{2.52}$$

$$\frac{\partial \tilde{r}_{m-2}}{\partial t} - c_n\frac{\partial \tilde{r}_{m-2}}{\partial x} - ((m-1)\beta c_n)^{1/2}\tilde{v}_{m-1} = \frac{1}{\sqrt{2}c_n}\tilde{\mathcal{S}}_{m-2}^n(x,t) \tag{2.53}$$

$$\frac{\partial \tilde{v}_{m-1}}{\partial t} + (m\beta c_n)^{1/2}\tilde{q}_m - ((m-1)\beta c_n)^{1/2}\tilde{r}_{m-2} = 0. \tag{2.54}$$

We can profitably study free wave solutions of these equations by setting $\mathcal{S}_m^n \equiv 0$ and considering plane wave solutions travelling around the tropics of the form

$$\begin{pmatrix} \tilde{q}_m \\ \tilde{r}_m \\ \tilde{v}_m \end{pmatrix} = Re \begin{pmatrix} q_m \\ r_m \\ v_m \end{pmatrix} e^{i(kx-\omega t)}. \tag{2.55}$$

The first equation for $\tilde{q}_0$, (2.49) gives rise to the eastward propagating Kelvin waves discussed above. Substituting the plane wave solution into (2.49) results in a relationship between the wavenumber k and the frequency ω (called a dispersion relation) given by

$$\omega = c_n k \tag{2.56}$$

and a solution given by

$$q(x, y, t) = \cos\left(k(x - c_n t)\right)\phi_0^n(y) = \alpha_n \cos\left(k(x - c_n t)\right)e^{-(\beta y^2/2c)}, \tag{2.57}$$

where $\alpha_n = (\pi c_n/\beta)^{-1/4}$. Both r and v vanish, resulting in a solution in the original variables u, v, and (c_n rescaled) p given by

$$\begin{pmatrix} u \\ v \\ p \end{pmatrix} = \begin{pmatrix} 1 \\ 0 \\ 1 \end{pmatrix} \frac{1}{\sqrt{2}} \alpha_n \cos\left(k(x - c_n t)\right)e^{-(\beta y^2/2c_n)}. \tag{2.58}$$

We can see from the solution that Kelvin waves are symmetric about the equator and propagate with a phase speed $c_n = NH_T/n\pi$. Higher modes (i.e. larger values of n) result in slower waves. Typical values of $N \approx 0.01$ s^{-1} and tropospheric height $H_T \approx 16$ km result in a wave speed of $c_1 = 50$ ms^{-1}.

Substituting the plane wave solution into the 2×2 system for $\tilde{v}_0$ and $\tilde{q}_1$ (2.50)-(2.51) gives the dispersion relation

$$\omega^2 - c_n \omega k - \beta c = 0 \tag{2.59}$$

which has roots

$$\omega_{\pm} = \frac{c_n k}{2} \pm \frac{\sqrt{c_n^2\omega^2 + 4c_n\beta}}{2}. \tag{2.60}$$

Here r vanishes and the solutions for q and v are

$$q = \cos(kx - \omega_{\pm}t)\phi_1^n(y) = \alpha_n \left(\frac{2\beta}{c_n}\right)^{1/2} y\cos(kx - \omega_{\pm}t)e^{-(\beta y^2/2c_n)} \tag{2.61}$$

$$v = \frac{(\beta c_n)^{1/2}}{\omega_{\pm}}\sin(kx - \omega_{\pm}t)\phi_0^n(y) = \alpha_n\frac{(\beta c_n)^{1/2}}{\omega_{\pm}}\sin(kx - \omega_{\pm}t)e^{-(\beta y^2/2c_n)}, \tag{2.62}$$

where α_n is defined as above. In terms of the original variables, the solution is

$$\begin{pmatrix} u \\ v \\ p \end{pmatrix} = \alpha_n e^{-(\beta y^2/2c_n)} \begin{pmatrix} (\beta/c_n)^{1/2} y\cos(kx - \omega_{\pm}t) \\ ((\beta c_n)^{1/2}/\omega_{\pm})\sin(kx - \omega_{\pm}t) \\ (\beta/c_n)^{1/2} y\cos(kx - \omega_{\pm}t) \end{pmatrix}. \tag{2.63}$$

These waves are called Yanai waves, or mixed Rossby-gravity waves.

If we now substitute the plane wave solution into the 3×3 system, we obtain the following linear system:

$$\begin{bmatrix} -i\omega + ic_nk & 0 & -(m\beta c_n)^{1/2} \\ 0 & -i\omega - ic_nk & ((m-1)\beta c_n)^{1/2} \\ (m\beta c_n)^{1/2} & -((m-1)\beta c_n)^{1/2} & -i\omega \end{bmatrix} = \begin{pmatrix} \tilde{q}_m \\ \tilde{r}_{m-2} \\ \tilde{v}_{m-1} \end{pmatrix} = 0. \tag{2.64}$$

The dispersion relation here is given by the characteristic equation of the linear system:

$$\omega(\omega^2 - c_n^2k^2) - \beta c_n((2m-1)\omega + c_nk) = 0, \tag{2.65}$$

which can be rewritten as

$$\left(\frac{\omega}{c_n}\right)^2 - k^2 - \frac{\beta}{\omega}k = \frac{\beta}{c_n}(2m-1), \tag{2.66}$$

since $\omega \neq 0$. For small ω/c, the solution is

$$\omega(k) \approx -\frac{\beta k}{(\beta/c_n)(2m-1) + k^2} \tag{2.67}$$

and for small $\beta k/\omega$, the solution is

$$\omega_{\pm}(k) \approx \pm\sqrt{c_n^2 k^2 + c_n\beta(2m-1)}, \tag{2.68}$$

where $m = 2, 3, \ldots$ in both cases. The first case is known as an equatorial Rossby wave (also called an equatorial planetary wave) and the second case is called an equatorial gravity wave. The eigenvectors associated with this problem are

$$\tilde{q}_m = i\frac{(m\beta c_n)^{1/2}}{\omega - c_n k}\tilde{v}_{m-1}, \quad \tilde{r}_{m-2} = -i\frac{((m-1)\beta c_n)^{1/2}}{\omega + c_n k}\tilde{v}_{m-1}, \tag{2.69}$$

and hence the solution in terms of q, r, and v is

$$\begin{pmatrix} q_m \\ r_{m-2} \\ v_{m-1} \end{pmatrix} = \begin{pmatrix} -\frac{(m\beta c_n)^{1/2}}{\omega - c_n k}\sin(kx - \omega t)\phi_m^n \\ \frac{((m-1)\beta c_n)^{1/2}}{\omega + c_n k}\sin(kw - \omega t)\phi_{m-2}^n \\ \cos(kx - \omega t)\phi_{m-1}^n \end{pmatrix}. \tag{2.70}$$

2.2 Barotropic Rossby Waves

When the linear primitive equations are averaged in the vertical direction, we obtain a PDE system for the barotropic mode $(\overline{\mathbf{v}}, \overline{p})$. Here we consider the linear barotropic mode alone, with no forcing terms:

$$\frac{\partial \overline{\mathbf{v}}}{\partial t} - \beta y \overline{\mathbf{v}}^{\perp} + \nabla \overline{p} = 0 \tag{2.71}$$

$$\nabla \cdot \overline{\mathbf{v}} = 0 \tag{2.72}$$

If we take the curl of the first equation, we get

$$\frac{\partial^2 \overline{v}}{\partial x \partial t} - \frac{\partial^2 \overline{u}}{\partial y \partial t} - \beta y\left(\frac{\partial \overline{u}}{\partial x} + \frac{\partial \overline{v}}{\partial y}\right) + \beta \overline{v} = 0. \tag{2.73}$$

Introducing the vorticity $\overline{\zeta}$ defined by

$$\overline{\zeta}(x, y, t) = \frac{\partial \overline{v}}{\partial x} - \frac{\partial \overline{u}}{\partial y} \tag{2.74}$$

and the streamfunction $\overline{\psi}$ defined by

$$\overline{u} = -\frac{\partial \overline{\psi}}{\partial y}, \qquad \overline{v} = \frac{\partial \overline{\psi}}{\partial x} \tag{2.75}$$

and using the incompressible constraint, we obtain

$$\frac{\partial \overline{\zeta}}{\partial t} + \beta \frac{\partial \overline{\psi}}{\partial x} = 0. \tag{2.76}$$

We may actually write this as an equation in the single variable $\overline{\psi}$ if we note that $\overline{\zeta} = \triangle \overline{\psi}$ and thus

$$\frac{\partial \triangle \overline{\psi}}{\partial t} + \beta \frac{\partial \overline{\psi}}{\partial x} = 0. \tag{2.77}$$

Searching for solutions of the form

$$\overline{\psi} \propto Re\left\{e^{i(kx+ly-\omega t)}\right\}, \tag{2.78}$$

we obtain

$$\omega(k,l) = -\frac{\beta k}{k^2 + l^2}, \tag{2.79}$$

which is the dispersion relation for the barotropic planetary waves, or Rossby waves, on an equatorial β-plane.

2.3 Galerkin Projection of the Nonlinear Evolution Equation

As Majda and Biello [16] have pointed out, a model involving a barotropic mode and a first baroclinic mode can capture important nonlinear equatorial interactions. First, we shall nondimensionalize the system using some characteristic scales. For the velocity scale, we choose the gravity wave speed $c = NH_T/\pi \approx 50$ m/s. A natural length scale choice is based on the equatorial Rossby wave deformation radius $L = (c/\beta)^{1/2} \approx 1500$ km. This leads to a time scale of $T = L/c \approx$

8 hours.

Armed with the knowledge gained from the study of the linearized version of the primitive equations, we can define a Galerkin projection of the first baroclinic mode using the function found in the separable solutions which resulted in vertical decoupling. Hence, we define an inner product $\langle f, g \rangle$ by

$$\langle f, g \rangle = \frac{1}{H_T} \int_0^{H_T} f(z) g(z) dz. \tag{2.80}$$

The result of the projection is that we may now reduce the dimension of the problem by one. We approximate the variables of velocity, pressure, and potential temperature as

$$\begin{pmatrix} \mathbf{V} \\ P \end{pmatrix} (x, y, z, t) \approx \begin{pmatrix} \overline{\mathbf{v}} \\ \overline{p} \end{pmatrix} (x, y, t) + \begin{pmatrix} \mathbf{v} \\ p \end{pmatrix} \cos\left(\frac{\pi z}{H_T}\right) \tag{2.81}$$

$$\begin{pmatrix} W \\ \Theta \end{pmatrix} (x, y, z, t) \approx \begin{pmatrix} \omega \\ \theta \end{pmatrix} (x, y, t) \sin\left(\frac{\pi z}{H_T}\right). \tag{2.82}$$

Using the Galerkin projection and functional inner product, noting that the vertical velocity can be expressed as a function of $\mathbf{v}$ using $w = -(\frac{H_T}{\pi})\nabla \cdot \mathbf{v}$ and the baroclinic pressure is related to the potential temperature by $p = -(gH_T\theta/\pi\theta_0)$, we find the resulting nonlinear interacting system [16]:

$$\frac{\partial \overline{\mathbf{v}}}{\partial t} + \overline{\mathbf{v}} \cdot \nabla \overline{\mathbf{v}} + y\overline{\mathbf{v}}^{\perp} + \nabla \overline{p} = -\frac{1}{2}(\mathbf{v} \cdot \nabla \mathbf{v} + \mathbf{v} \nabla \cdot \mathbf{v}) \tag{2.83}$$

$$\nabla \cdot \overline{\mathbf{v}} = 0. \tag{2.84}$$

$$\frac{\partial \mathbf{v}}{\partial t} + \overline{\mathbf{v}} \cdot \nabla \mathbf{v} - \nabla \theta + y\mathbf{v}^{\perp} = -\mathbf{v} \cdot \nabla \overline{\mathbf{v}} \tag{2.85}$$

$$\frac{\partial \theta}{\partial t} + \overline{\mathbf{v}} \cdot \nabla \theta - \nabla \cdot \mathbf{v} = \mathcal{S}_{\Theta}(x, y, t) \tag{2.86}$$

If we wish to study only the barotropic response to a baroclinic forcing, we may do so using the first two equations of this system. We can consider the right hand side

of the first equation, $-\frac{1}{2}(\mathbf{v}\cdot\nabla\mathbf{v}+\mathbf{v}\nabla\cdot\mathbf{v})$, to be just such a baroclinic forcing. At this point, it is useful to introduce the potential vorticity-streamfunction formulation for barotropic waves. Let the potential vorticity $\overline{\xi}$ and the streamfunction $\overline{\psi}$ be defined as

$$\overline{\xi} = \frac{\partial \overline{v}}{\partial x} - \frac{\partial \overline{u}}{\partial y} + y \tag{2.87}$$

$$\overline{u} = -\frac{\partial \overline{\psi}}{\partial y}, \quad \overline{v} = \frac{\partial \overline{\psi}}{\partial x}. \tag{2.88}$$

Writing the interacting system in vorticity-streamfunction form gives:

$$\frac{\partial \overline{\xi}}{\partial t} + \overline{u}\frac{\partial \overline{\xi}}{\partial x} + \overline{v}\frac{\partial \overline{\xi}}{\partial y} = f(x,y,t) \quad \text{or} \tag{2.89}$$

$$\frac{\partial \overline{\xi}}{\partial t} + J(\overline{\psi},\overline{\xi}) = f(x,y,t)$$

$$\triangle\overline{\psi} = \overline{\xi} - y \tag{2.90}$$

$$\overline{u} = -\frac{\partial \overline{\psi}}{\partial y}, \quad \overline{v} = \frac{\partial \overline{\psi}}{\partial x} \tag{2.91}$$

$$f(x,y,t) = -\frac{1}{2}\left(\nabla \times [(\mathbf{v}\cdot\nabla\mathbf{v} + \mathbf{v}\nabla\cdot\mathbf{v})\ \hat{\mathbf{k}}]\right), \tag{2.92}$$

where $J(\overline{\psi},\overline{\xi})$ represents the Jacobian determinant of $\overline{\psi}$ and $\overline{\xi}$, and $\hat{\mathbf{k}}$ is the upward normal unit vector. We may think of the function $f(x,y,t)$ as a forcing of the right-hand side of the first equation. With $f \equiv 0$, this equation is the free nonlinear barotropic vorticity equation. Since the Jacobian determinant of the plane Rossby waves in (2.78) and (2.79) vanishes, the latter are also solutions for this nonlinear systems. These solutions will be used below to validate and assess the numerical methods utilized here.

Chapter 3

Numerical Methods

The barotropic vorticity equation (2.89) for two dimensional incompressible flow play a central role in what is to follow. These equations were used to make the first successful numerical weather predictions in the early 1950s. In our study of tropical climate dynamics, we shall be concerned with atmospheric motion close to the equator. The physical basis for using this equation to study the tropical climate was developed above. Now we develop numerical methods used to solve the equation. In the absence of forcing, the normalized version of the barotropic vorticity equation for equatorial motion is given by:

$$\frac{\partial \xi}{\partial t} + \mathbf{v} \cdot \nabla \xi = 0 \tag{3.1}$$

$$\triangle \psi = \xi - y \tag{3.2}$$

$$u = -\frac{\partial \psi}{\partial y}; \quad v = \frac{\partial \psi}{\partial x}. \tag{3.3}$$

Here $u = u(x, y)$ and $v = v(x, y)$ are known as the zonal (in east-west or x-direction) and meridional (in north-south or y-direction) velocities, respectively,

$\xi = \xi(x, y)$ is the potential vorticity, $\psi = \psi(x, y)$ is the stream function, and $\triangle$ is the Laplacian operator in two dimensions given by $\triangle\psi = \frac{\partial^2\psi}{\partial x^2} + \frac{\partial^2\psi}{\partial y^2}$. (We omit the overbars here since all velocities are barotropic, or z independent.) For our problem, we will restrict the domain to be a rectangular strip which is periodic in x. This domain is centred on the equator and represents the tropics, our principal region of interest.

3.1 Finite Differences

The standard way to solve a differential equation numerically is to discretize the domain, all functions of interest within the domain, and their derivatives using finite differences. We represent a continuous interval $(0, L)$ by dividing it into n equal pieces, each of length $h = L/n$. A function $f(x)$ defined on the entire interval $(0, L)$ can be represented by its values at each of the $n+1$ grid points $x_i = ih$ ($i = 0, 1, \ldots, n$). These discretizations generalize to higher dimensions. Derivatives are approximated by finite differences, based on a Taylor series expansion. One such method, the forward differencing scheme, uses the Taylor series

$$f'(x) = \frac{f(x+h) - f(x)}{h} + O(h) \tag{3.4}$$

to define an approximate derivative for each grid point

$$f'(x_i) \simeq \frac{f(x_{i+1}) - f(x_i)}{h}, \tag{3.5}$$

where the discrete derivative has an error of order $O(h)$ due to the truncation of the Taylor series. Here, we say an error is of order $O(h)$ if the error is bounded by Mh for some constant $M > 0$. The forward differencing scheme (3.5) is said to be first order accurate, based on the order of the truncation error. Using this approach, a linear differential equation may be approximated as a finite linear system and

solved using the methods of linear algebra. Solving large linear systems can be very time consuming and therefore it is important to consider other methods which may be available due to the features of the problem to be solved. The most widely used numerical methods for solving differentially equations for practical applications involve the use of Fast Fourier Transforms (FFTs). We shall develop these methods for Poisson's equation (3.2), which must be solved as part of (3.1)-(3.3).

3.2 Poisson's Equation

We would like to solve Poisson's equation on a 2-dimensional x-periodic domain $D = [0, L] \times [-Y, Y]$:

$$\triangle\psi(x, y) = \zeta(x, y), \tag{3.6}$$

$$\psi(0, y) = \psi(L, y), \tag{3.7}$$

$$\zeta(0, y) = \zeta(L, y), \tag{3.8}$$

where $\zeta(x, y) = \xi(x, y) - y$. We may represent the 2-dimensional Laplacian using centred finite differences as

$$\triangle\psi_{i,j} \simeq \frac{\psi_{i+1,j} - 2\psi_{i,j} + \psi_{i-1,j}}{(\Delta x)^2} + \frac{\psi_{i,j+1} - 2\psi_{i,j} + \psi_{i,j-1}}{(\Delta y)^2} = \zeta_{i,j}, \tag{3.9}$$

where $\Delta x = L/n$ and $\Delta y = 2Y/m$ for an $n \times m$ grid. This finite difference is second order in both spatial directions. The resulting linear system is given by $A\vec{\psi} = \vec{\zeta}$, where the coefficient matrix A is block tridiagonal of dimension $(n \times m)^2$ and $\vec{\psi}$ and $\vec{\zeta}$ have been reordered into vectors of length $m \times n$. Increasing the number of grid points will result in a more accurate approximation but will greatly increase the size of the coefficient matrix that must be inverted to solve the associated linear system. Using the traditional method of Gaussian elimination requires, in

general, on the order of $O(n^3)$ operations to solve an $n \times n$ linear system [6]. For a sparse matrix like this one, with a small proportion of nonzero entries, there are often factorings which can reduce the number of operations, and hence, the total computational time required.

Another approach is to use an iterative method. For example, the n-dimensional linear system $A\vec{x} = \vec{b}$ may be solved by the method of successive overrelaxation (SOR) by defining the $(k+1)^{th}$ iterate by

$$x_i^{(k+1)} = x_i^{(k)} + \omega \left(\hat{x}_i^{(k+1)} - x_i^{(k)} \right), \tag{3.10}$$

where $\omega \in (0, 2)$ and $\hat{x}_i^k$ is the k^{th} Gauss-Seidel iterate given by

$$\hat{x}_i^{(k+1)} = \frac{1}{a_{ii}} \left(b_i - \sum_{j<i} a_{ij} x_j^{(k+1)} - \sum_{j>i} a_{ij} x_j^{(k)} \right). \tag{3.11}$$

Here $a_{i,j}$ is the $(i,j)^{th}$ entry of A and b_j is the j^{th} entry of $\vec{b}$. We require that $a_{ii} \neq 0$ and that A be a positive-definite and symmetric (i.e. $a_{ij} = a_{ji}, \quad \forall i, j \quad \vec{x}^T \mathrm{A} \vec{x} > 0 \quad \forall \vec{x} \neq 0$). If these conditions are met, then the SOR iterates are guaranteed to converge to the unique solution of the linear system $A\vec{x} = \vec{b}$. For the SOR method, the number of operations per iteration is $O(4n + 2cn)$, where c is the average number of elements per row and the rate of convergence is dependent upon choosing the optimum value for ω. For large, sparse systems, the SOR method outperforms any direct methods [6].

While the SOR method may be the best general method for solving a linear system, using a spectral method is more suited to our problem. The idea behind a spectral method is to use a truncated series of orthogonal functions in order to represent the functions of interest for our problem. Due to the speed of Fast Fourier Transforms (FFT) algorithms [20], the discrete version of the Fourier transform has become a very useful and versatile method.

The discrete Fourier transform (DFT) with respect to x of a function $u(x, y)$ is defined as

$$\mathcal{F}(u_{j,k}) = \tilde{u}_{l,k} = \sum_{j=0}^{n-1} u_{j,k} e^{-i2\pi jl/n}, \tag{3.12}$$

and the inverse discrete Fourier transform,

$$\mathcal{F}^{-1}(\tilde{u}_{l,k}) = u_{j,k} = \frac{1}{n} \sum_{l=0}^{n-1} \tilde{u}_{l,k} e^{i2\pi jl/n}. \tag{3.13}$$

An approximation of the second derivative of a function $u(x)$ can be represented using the DFT as

$$\mathcal{F}\{u''_{j,k}\} \simeq \lambda_k \tilde{u}_{l,k}, \quad \lambda_k = \frac{2(\cos(2\pi l/n) - 1)}{(\Delta x)^2}. \tag{3.14}$$

We can use this representation to transform Poisson's equation into a second order ordinary differential equation:

$$\lambda_k \tilde{\psi}_{l,k} + \frac{\tilde{\psi}_{l,k+1} - 2\tilde{\psi}_{l,k} + \tilde{\psi}_{l,k-1}}{(\Delta y)^2} = \tilde{\zeta}_{l,k}, \tag{3.15}$$

or equivalently

$$\tilde{\psi}_{l,k+1} + (\lambda_k (\Delta y)^2 - 2)\tilde{\psi}_{l,k} + \tilde{\psi}_{l,k-1} = (\Delta y)^2 \tilde{\zeta}_{l,k}. \tag{3.16}$$

This tridiagonal system can be solved easily using the (transformed) boundary conditions. A subsequent application of the inverse DFT yields the solution to Poisson's equation. Using the FFT algorithm, originally developed by Cooley and Tukey, to compute the DFT takes only $O(n)$ operations. A tridiagonal system can be solved in $O(n)$ operations. Hence, the semi-spectral method represents a substantial improvement over both the direct and the iterative methods discussed above.

Armed with an efficient method of solving Poisson's equation for each time step, it remains to solve the free barotropic vorticity equation. Care must be taken, as certain seemingly natural discretizations can lead to computational instabilities.

3.3 Free Equatorial Barotropic Vorticity Equation

The free equatorial barotropic vorticity equation can be written in three equivalent ways. Up until now, we have only considered the advective form:

$$\frac{\partial \xi}{\partial t} + u\frac{\partial \xi}{\partial x} + v\frac{\partial \xi}{\partial y} = 0. \tag{3.17}$$

A central feature of the barotropic vorticity equation is the fact that potential vorticity is advected, or transported, through the flow. Even though it is simple to code, this form is not typically used in practice in part because it does not have any obvious conservative properties and hence, can more easily result in instabilities which grow with each time step. We shall discuss this more below. An attractive alternative uses the incompressibility of the velocity field to write the equation in a flux form:

$$\frac{\partial \xi}{\partial t} + \nabla \cdot (\mathbf{v}\xi) = 0. \tag{3.18}$$

This flux form is a conservation law in the sense that the local rate of change of ξ is determined by the flux of $\mathbf{v}\xi$. Despite the advantages of using a conservation law, such a method may allow solutions that contain shocks or discontinuities. The combination of a conservation law and piecewise-constant initial data containing a discontinuity (called a Riemann problem) can lead to a solution in which the discontinuity propagates with time. This will lead to computational instabilities. Khouider and Majda [8] adapted a central scheme [14] using both the advective and conservative forms (3.17)-(3.18) to avoid this problem. A piecewise approximation at each time step using staggered averaging results in smooth numerical fluxes, thereby avoiding discontinuous Riemann fans. (While we wish to avoid the difficult issues associated with Riemann problems by using a different numerical scheme, one may learn of the challenges of modelling propagating shock waves

and Riemann fans in [2].) This method is used for validation of code based on the third form, which is a Jacobian form:

$$\frac{\partial \xi}{\partial t} + J(\psi, \xi) = 0, \quad J(\psi, \xi) = \frac{\partial \psi}{\partial x}\frac{\partial \xi}{\partial y} - \frac{\partial \xi}{\partial x}\frac{\partial \psi}{\partial y}. \tag{3.19}$$

Many early attempts to solve the barotropic vorticity equation used the Jacobian formulation. The main reason for this is because under certain conditions, this Jacobian has the useful feature that both domain integrated enstrophy (one-half the square of the vorticity) and domain integrated kinetic energy are conserved. We will now examine this result, first shown by Fjørtoft, before discussing a certain type of instability and Arakawa's method of dealing with this problem.

3.4 Jacobian for 2-D Incompressible Flow

We start with the non-rotating barotropic vorticity equation

$$\frac{\partial \zeta}{\partial t} + J(\psi, \zeta) = 0. \tag{3.20}$$

For simplicity, we will work with the vorticity $\zeta = \frac{\partial v}{\partial x} - \frac{\partial u}{\partial y}$ rather than the potential vorticity ξ defined in (2.87). Analogous results may be obtained using the potential vorticity. Fjørtoft showed that given smooth initial conditions, solutions remain smooth in the sense that there can be no net transfer of energy from large scales to small scales [3]. This can be seen by examining the domain integral of the Jacobian operator. Suppose the spatial domain D is rectangular and either periodic or, alternatively, the normal velocity vanishes at the boundary ∂D. Let $\overline{p}$ denote the domain integral of p:

$$\overline{p(x,y)} = \int\int_D p dx dy. \tag{3.21}$$

Consider the domain integral of $J(a, b)$, for suitably well behaved functions $a(x, y)$ and $b(x, y)$:

$$\overline{J(a,b)} = \overline{\frac{\partial}{\partial x}\left(a\frac{\partial b}{\partial y}\right)} - \overline{\frac{\partial}{\partial y}\left(a\frac{\partial b}{\partial x}\right)} = 0, \tag{3.22}$$

where we used that fact that $\int \frac{\partial}{\partial x}\left(a\frac{\partial b}{\partial y}\right)dx$ vanishes due to the periodicity of the domain. This result implies that

$$\overline{aJ(a,b)} = \overline{a\frac{\partial}{\partial x}\left(a\frac{\partial b}{\partial y}\right)} - \overline{a\frac{\partial}{\partial y}\left(a\frac{\partial b}{\partial x}\right)} = \overline{J(a^2/2,b)} = 0, \tag{3.23}$$

and similarly

$$\overline{bJ(a,b)} = \overline{b\frac{\partial}{\partial x}\left(a\frac{\partial b}{\partial y}\right)} - \overline{b\frac{\partial}{\partial y}\left(a\frac{\partial b}{\partial x}\right)} = \overline{J(a,b^2/2)} = 0. \tag{3.24}$$

One implication of this concerns the enstrophy, which is usually defined as $\zeta^2/2$ (*i.e.* one-half the square of the vorticity). Noting that $\zeta^2/2 = (\triangle\psi)^2/2$, we may multiply the BVE by $\triangle\psi$ and integrate over the domain to obtain

$$\frac{\partial}{\partial t}\left(\overline{\frac{(\triangle\psi)^2}{2}}\right) + \overline{(\triangle\psi)J(\psi,\triangle\psi)} = 0, \tag{3.25}$$

which implies

$$\frac{\partial}{\partial t}\left(\overline{\frac{(\triangle\psi)^2}{2}}\right) = 0. \tag{3.26}$$

Hence, the domain-integrated enstrophy is conserved. Now consider the kinetic energy, defined as $\mathbf{v}\cdot\mathbf{v}/2$. Multiplying the BVE by the stream function ψ yields

$$\psi\frac{\partial\zeta}{\partial t} = -\psi\nabla\cdot(\mathbf{v}\zeta) = -\nabla\cdot(\mathbf{v}\zeta\psi) + \zeta\mathbf{v}\cdot\nabla\psi, \tag{3.27}$$

where we have made use of the vector identity $\nabla\cdot(\lambda\mathbf{a}) = \nabla\lambda\cdot\mathbf{a} + \lambda(\nabla\cdot\mathbf{a})$. Note that the second term on the right-hand side above vanishes due to the fact that $\mathbf{v}$ is perpendicular to $\nabla\psi$ by definition. With some straightforward manipulation, the right-hand side becomes

$$\psi\frac{\partial\zeta}{\partial t} = \psi\frac{\partial\triangle\psi}{\partial t} = \frac{\partial(\nabla\psi\cdot\nabla\psi)}{\partial t} - \nabla\psi\cdot\frac{\partial\nabla\psi}{\partial t} = \frac{\partial(\mathbf{v}\cdot\mathbf{v})}{\partial t} - \frac{\partial(\mathbf{v}\cdot\mathbf{v}/2)}{\partial t} = \frac{\partial(\mathbf{v}\cdot\mathbf{v}/2)}{\partial t}. \tag{3.28}$$

Hence, we have

$$\frac{\partial(\mathbf{v}\cdot\mathbf{v}/2)}{\partial t} = -\nabla\cdot(\mathbf{v}\zeta\psi), \tag{3.29}$$

which, when integrated over the entire domain, gives

$$\frac{\partial(\overline{\mathbf{v}\cdot\mathbf{v}/2})}{\partial t} = 0. \tag{3.30}$$

Therefore, the domain-integrated kinetic energy is conserved. A useful consequence of these conservation results may be derived by first expanding the stream function in a double Fourier series along the x and y coordinates:

$$\psi = \sum_k \sum_l a_{k,l} e^{i(kx+ly)} = \sum_{k,l} \psi_{k,l}, \tag{3.31}$$

where the $a_{k,l}$ are real numbers representing the coefficients of the Fourier expansion. Define a total wave number κ such that $\kappa^2 = k^2 + l^2$. Then

$$\overline{\mathbf{v}\cdot\mathbf{v}} = \overline{\nabla\psi\cdot\nabla\psi} = \overline{\nabla\cdot(\psi\nabla\psi)} - \overline{\psi\triangle\psi} = -\overline{\psi\triangle\psi} = \sum_{k,l} \kappa^2 \overline{\psi_{k,l}^2}, \tag{3.32}$$

where we have used the periodicity of the domain and the fact that the Fourier modes are mutually orthogonal. Furthermore,

$$\overline{\zeta^2} = \overline{(\triangle\psi)^2} = \sum_{k,l} \kappa^4 \overline{\psi_{k,l}^2}. \tag{3.33}$$

An average wave number κ_{avg} may now be defined using the relations above:

$$\kappa_{avg} = \left(\frac{\overline{\zeta^2}}{\overline{\mathbf{v}\cdot\mathbf{v}}} \right)^{1/2}. \tag{3.34}$$

Since we have already showed that both the domain-integrated enstrophy and the domain-integrated kinetic energy are conserved, κ_{avg} does not change with time. This implies that there can be no systematic energy cascades, *i.e.* no net transfer of energy from larger (smaller) scales to smaller (larger) scales. More explicitly, only the following energy exchanges are possible:

$$K_L \leftarrow K_M \rightarrow K_S, \tag{3.35}$$

or

$$K_L \rightarrow K_M \leftarrow K_S, \tag{3.36}$$

where K_L, K_M, and K_S are the mean kinetic energies of the long, medium, and short waves, respectively.

3.5 Computational Instabilities

We have just shown that, under certain conditions, the BVE written in the Jacobian formulation has some nice conservation properties. It is only natural to desire the same conservation properties in a discretization of the Jacobian. An intuitive way to discretize the Jacobian would be to use centred differences to approximate as

$$J_1(\psi, \zeta) = \frac{\partial \psi}{\partial x}\frac{\partial \zeta}{\partial y} - \frac{\partial \psi}{\partial y}\frac{\partial \zeta}{\partial x}. \tag{3.37}$$

This requires a five point stencil, as displayed in Figure 1. However, it was noted in

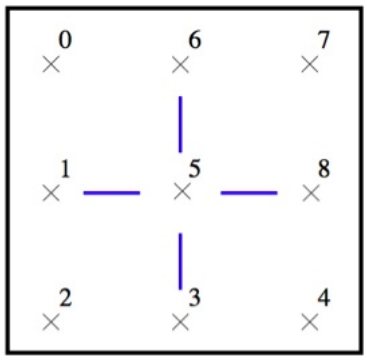

Figure 3.1: Five point stencil for centred differences Jacobian

the late 1950s by Phillips [19] that this scheme is subject to instabilities stemming from the misrepresentation of wavelengths shorter than about two grid intervals. Such wavelengths, formed by the nonlinear interaction of longer waves, get misrepresented as long waves. An example of this phenomenon can be seen in Figure 3.2, where the period of a sine wave is erroneously represented. This misrepresentation, also called aliasing, is not due to a poor choice of boundary conditions or to an inappropriately large time step but is rather an inherent feature (or shortcoming) of the scheme. The instabilities resulting from aliasing can grow without bound in a finite amount of time. Phillips showed that such instabilities

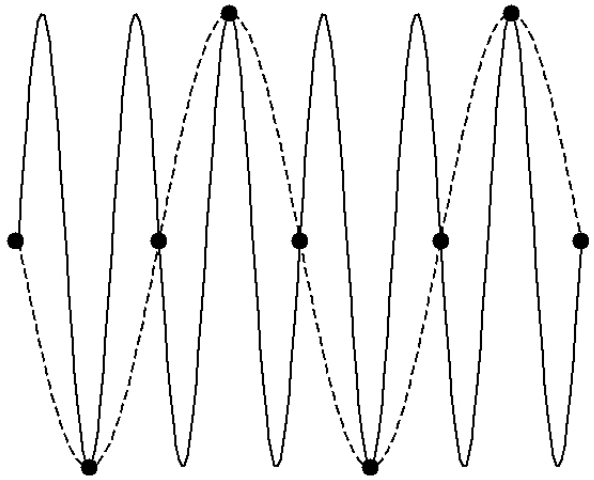

Figure 3.2: Misrepresentation of $f(x) = \sin(3x)$ as $f(x) = -\sin(x)$ due to aliasing.

can be eliminated if all waves with wavelengths shorter than four grid intervals are removed.

3.6 Arakawa Jacobian

However, alternative discretizations would result from the using either of the following:

$$J_2(\psi,\zeta) = \frac{\partial}{\partial x}\left(\psi\frac{\partial\zeta}{\partial y}\right) - \frac{\partial}{\partial y}\left(\psi\frac{\partial\zeta}{\partial x}\right), \tag{3.38}$$

$$J_3(\psi,\zeta) = \frac{\partial}{\partial y}\left(\zeta\frac{\partial\psi}{\partial x}\right) - \frac{\partial}{\partial x}\left(\zeta\frac{\partial\psi}{\partial y}\right). \tag{3.39}$$

In early attempts to make numerical weather predictions, J_1 was usually used. We define a discretized analogue of J_1 by

$$J^{++}_{i,j}(\psi,\zeta) = \frac{(\psi_{i+1,j}-\psi_{i-1,j})(\zeta_{i,j+1}-\zeta_{i,j-1}) - (\zeta_{i+1,j}-\zeta_{i-1,j})(\psi_{i,j+1}-\psi_{i,j-1})}{4d^2}, \tag{3.40}$$

where for simplicity, we have made the spatial discretization uniform, *i.e.* $\Delta x = \Delta y = d$.

A more natural method of eliminating instabilities and stabilizing the solution was proposed by Arakawa in 1966 [1]. Using a judicious combination of J_1, J_2, and J_3, Arakawa was able to propose a discrete Jacobian that conserved the numerical analogues of the domain-integrated kinetic energy, domain-integrated enstrophy, and average wave number.

Here we define the discrete analogues of J_2 and J_3 as $J^{+\times}$ and $J^{\times+}$ respectively:

$$J^{+\times}_{i,j}(\psi,\zeta) = (1/4d^2)[\psi_{i+1,j}(\zeta_{i+1,j+1} - \zeta_{i+1,j-1}) - \psi_{i-1,j}(\zeta_{i-1,j+1} - \zeta_{i-1,j-1}) \\ -\psi_{i,j+1}(\zeta_{i+1,j+1} - \zeta_{i-1,j+1}) + \psi_{i,j-1}(\zeta_{i+1,j-1} - \zeta_{i-1,j-1})] \tag{3.41}$$

$$J^{\times+}_{i,j}(\psi,\zeta) = (1/4d^2)[\zeta_{i,j+1}(\psi_{i+1,j+1} - \psi_{i-1,j+1}) - \zeta_{i,j-1}(\psi_{i+1,j-1} - \psi_{i-1,j-1}) \tag{3.42}$$

$$-\zeta_{i+1,j}(\psi_{i+1,j+1} - \psi_{i+1,j-1}) + \zeta_{i-1,j}(\psi_{i-1,j+1} - \psi_{i-1,j-1})] \tag{3.43}$$

As can be seen from the figure below, a nine point stencil is required for this Jacobian. In other words, calculation of the Jacobian at grid point number five in the diagrams requires information from all eight adjacent grid points, not just the four used for the centred differences Jacobian. Writing the finite difference analogue of the Jacobian in the most general form

$$J_{i,j}(\psi,\zeta) = \sum_{i',j'}\sum_{i'',j''} c_{i,j;i',j';i'',j''}\zeta_{i+i',j+j'}\psi_{i+i'',j+j''}, \tag{3.44}$$

where $\zeta_{i+i',j+j'}$ is the vorticity at a neighbouring grid point $(i+i', j+j')$ and $\psi_{i+i'',j+j''}$ is the stream function at a neighbouring grid point $(i+i'', j+j'')$. Now if we define a linear combination of velocity components by finite differences of the stream function

$$a_{i,j;i+i',j+j'} \equiv \sum_{i'',j''} c_{i,j;i',j';i'',j''}\psi_{i+i'',j+j''}, \tag{3.45}$$

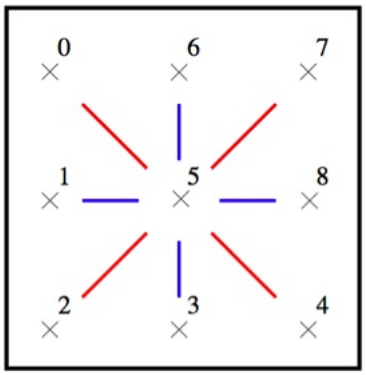

Figure 3.3: Nine point stencil for centred differences Jacobian

and multiply by $\zeta_{i,j}$, we obtain

$$\zeta_{i,j} J_{i,j}(\psi, \zeta) = \sum_{i',j'} a_{i,j;i+i',j+j'} \zeta_{i,j} \zeta_{i+i',j+j'}. \tag{3.46}$$

The left side of this equation is the time change of enstrophy due to advection. Therefore, the term $a_{i,j;i+i',j+j'} \zeta_{i,j} \zeta_{i+i',j+j'}$ can be interpreted as the enstrophy gain at the grid point (i, j) due to interaction with the grid point $(i + i', j + j')$. Similarly, we may interpret the term $a_{i+i',j+j';i,j} \zeta_{i+i',j+j'} \zeta_{i,j}$ as the enstrophy gain at the grid point $(i + i', j + j')$ due to interaction with the grid point (i, j). We require that these quantities have equal magnitude and opposite sign, irrespective of $\zeta_{i,j}$ and $\zeta_{i+i',j+j'}$, so that false production of enstrophy is avoided. This implies that

$$a_{i+i',j+j';i,j} = -a_{i,j;i+i',j+j'}. \tag{3.47}$$

Consider again the general formulation of the finite difference Jacobian as a linear combination of $J^{++}_{i,j}$, $J^{+\times}_{i,j}$, and $J^{\times+}_{i,j}$:

$$J_{i,j}(\psi, \zeta) = \alpha J^{++}_{i,j}(\psi, \zeta) + \beta J^{+\times}_{i,j}(\psi, \zeta) + \gamma J^{\times+}_{i,j}(\psi, \zeta), \tag{3.48}$$

where $\alpha + \beta + \gamma = 1$. Using this linear combination, we calculate the following

coefficients representing interactions of the grid point (i, j) with its neighbours:

$$a_{i,j;i+1,j} = (1/4d^2)[-\alpha(\psi_{i,j+1} - \psi_{i,j-1}) - \gamma(\psi_{i+1,j+1} - \psi_{i+1,j-1})], \tag{3.49}$$

$$a_{i,j;i-1,j} = (1/4d^2)[\alpha(\psi_{i,j+1} - \psi_{i,j-1}) + \gamma(\psi_{i-1,j+1} - \psi_{i-1,j-1})], \tag{3.50}$$

$$a_{i,j;i,j+1} = (1/4d^2)[\alpha(\psi_{i+1,j} - \psi_{i-1,j}) + \gamma(\psi_{i+1,j+1} - \psi_{i-1,j+1})], \tag{3.51}$$

$$a_{i,j;i,j-1} = (1/4d^2)[-\alpha(\psi_{i+1,j} - \psi_{i-1,j}) - \gamma(\psi_{i+1,j-1} - \psi_{i-1,j-1})], \tag{3.52}$$

$$a_{i,j;i+1,j+1} = (1/4d^2)[\beta(\psi_{i+1,j} - \psi_{i,j+1})], \tag{3.53}$$

$$a_{i,j;i-1,j-1} = (1/4d^2)[\beta(\psi_{i-1,j} - \psi_{i,j-1})], \tag{3.54}$$

$$a_{i,j;i-1,j+1} = (1/4d^2)[\beta(\psi_{i,j+1} - \psi_{i-1,j})], \tag{3.55}$$

$$a_{i,j;i+1,j-1} = (1/4d^2)[\beta(\psi_{i,j-1} - \psi_{i+1,j})]. \tag{3.56}$$

From these equations, we can derive a subsequent set of equations for the interaction of neighbouring grid points with the grid point (i,j):

$$a_{i+1,j;i,j} = (1/4d^2)[\alpha(\psi_{i+1,j+1} - \psi_{i+1,j-1}) + \gamma(\psi_{i,j+1} - \psi_{i,j-1})], \tag{3.57}$$

$$a_{i-1,j;i,j} = (1/4d^2)[-\alpha(\psi_{i-1,j+1} - \psi_{i-1,j-1}) - \gamma(\psi_{i,j+1} - \psi_{i,j-1})], \tag{3.58}$$

$$a_{i,j+1;i,j} = (1/4d^2)[-\alpha(\psi_{i+1,j+1} - \psi_{i-1,j+1}) - \gamma(\psi_{i+1,j} - \psi_{i-1,j})], \tag{3.59}$$

$$a_{i,j-1;i,j} = (1/4d^2)[\alpha(\psi_{i+1,j-1} - \psi_{i-1,j-1}) + \gamma(\psi_{i+1,j} - \psi_{i-1,j})], \tag{3.60}$$

$$a_{i-1,j-1;i,j} = (1/4d^2)[\beta(\psi_{i,j-1} - \psi_{i-1,j})], \tag{3.61}$$

$$a_{i+1,j+1;i,j} = (1/4d^2)[\beta(\psi_{i,j+1} - \psi_{i+1,j})], \tag{3.62}$$

$$a_{i+1,j-1;i,j} = (1/4d^2)[\beta(\psi_{i+1,j} - \psi_{i,j-1})], \tag{3.63}$$

$$a_{i-1,j+1;i,j} = (1/4d^2)[\beta(\psi_{i-1,j} - \psi_{i,j+1})]. \tag{3.64}$$

These two sets of equations, together with the constraint (3.47), imply that for an enstrophy conserving scheme, we require $\alpha = \gamma$. Hence, any scheme using the

Jacobian $\alpha(J^{++}_{i,j}(\psi,\zeta) + J^{\times+}_{i,j}(\psi,\zeta)) + \beta J^{+\times}_{i,j}(\psi,\zeta)$, where $2\alpha+\beta = 1$, will conserve enstrophy.

An analysis of conservation of kinetic energy between adjacent grid points may be performed analogously by considering the finite difference analogue of $\psi J(\psi,\zeta)$. This analysis requires that $\alpha = \beta$ in order for conservation of kinetic energy to hold. Therefore, the only possible scheme conserving both kinetic energy and enstrophy is one in which $\alpha = \beta = \gamma = \frac{1}{3}$. This scheme also conserves anti-symmetry, as can be shown a straightforward (though tedious) direct calculation. By using this so-called Arakawa Jacobian, one may avoid the instabilities found in other methods due to the built-in conservation properties. No adjustment or filtering for aliasing is required. A summary of conservation properties is contained in the table below.

$J(\psi,\zeta)$	J^{++}	$J^{\times+}$	$J^{+\times}$	$(J^{++}+J^{\times+}+J^{+\times})/3$
$J(\psi,\zeta) = -J(\zeta,\psi)$	$\surd$			$\surd$
K.E. conserved		$\surd$		$\surd$
Enstrophy conserved			$\surd$	$\surd$

Table 3.1: Comparison of conservation properties for various Jacobians.

3.7 Strang Splitting

We have discussed how to discretize the "free" BVE in some detail. When a forcing term $f(x,y,t)$ is introduced, *i.e.*

$$\frac{\partial \xi}{\partial t} + \mathbf{u}\cdot\nabla\xi = f(x,y,t), \tag{3.65}$$

the situation becomes a bit more complicated. We shall deal with forcing (or source) terms using a fractional step method referred to as splitting. The idea

is to break down the problem into distinct pieces, each of which is treated as its own independent problem. In this way, a numerical method appropriate for each subproblem may be designed and implemented without having to fuss about the ramifications the method will have on other subproblem(s).

For simplicity, consider the one-dimensional problem

$$\frac{\partial \xi(x,t)}{\partial t} = (\mathcal{A}+\mathcal{B})\xi(x,t), \tag{3.66}$$

where $\mathcal{A} = \mathcal{A}(x)$ and $\mathcal{B} = \mathcal{B}(x)$ are time independent (but may be differential operators). Note that

$$\frac{\partial^2 \xi}{\partial t^2} = (\mathcal{A}+\mathcal{B})\frac{\partial \xi}{\partial t} = (\mathcal{A}+\mathcal{B})^2\xi, \tag{3.67}$$

and in general

$$\frac{\partial^n \xi}{\partial t^n} = (\mathcal{A}+\mathcal{B})^n\xi. \tag{3.68}$$

Note that using a Taylor series expansion, we can write the solution after a time step $\Delta t = k$ as

$$\begin{aligned} \xi(x,k) &= \xi(x,0) + k(\mathcal{A}+\mathcal{B})\xi(x,0) + \frac{k^2}{2}(\mathcal{A}+\mathcal{B})^2\xi(x,0) + \dots \\ &= (I + k(\mathcal{A}+\mathcal{B}) + \frac{k^2}{2}(\mathcal{A}+\mathcal{B}) + \dots)\xi(x,0) \\ &= \sum_{j=0}^{\infty} \frac{k^j}{j!}(\mathcal{A}+\mathcal{B})^j\xi(x,0), \end{aligned} \tag{3.69}$$

which could also be written as

$$\xi(x,k) = e^{k(\mathcal{A}+\mathcal{B})}\xi(x,0). \tag{3.70}$$

The method of Strang splitting is to divide this problem into two subproblems [2]. The first subproblem,

$$\frac{\partial \xi}{\partial t} = \mathcal{A}\xi, \tag{3.71}$$

is solved over a half time step of length $k/2$. The result is then used as input for the second subproblem,

$$\frac{\partial \xi}{\partial t} = \mathcal{B}\xi, \tag{3.72}$$

which is solved over a full time step of length k. Finally, the first subproblem is solved on a half a time step, using the result of the second subproblem as an input. To analyze the error of this splitting method, we must calculate the difference between the exact solution $\xi(x,k)$ and the approximation $\xi^*(x,k)$ after one time step, we may be expressed as

$$\xi(x,k) - \xi^*(x,k) = \left(e^{k(\mathcal{A}+\mathcal{B})} - e^{k\mathcal{A}/2}e^{k\mathcal{B}}e^{k\mathcal{A}/2}\right)\xi(x,0), \tag{3.73}$$

where we note that $\mathcal{AB}$ does not necessarily equal $\mathcal{BA}$. Again using a Taylor series expansion, we have

$$\begin{aligned}\xi^*(x,k) &= \xi(x,0)\left(I + \frac{k}{2}\mathcal{A} + \frac{k^2}{8}\mathcal{A}^2 + \dots\right)\left(I + k\mathcal{B} + \frac{k^2}{2}\mathcal{B}^2 + \dots\right) \\ &\quad \left(I + \frac{k}{2}\mathcal{A} + \frac{k^2}{8}\mathcal{A}^2 + \dots\right) \\ &= \xi(x,0)\left(I + k(\mathcal{A}+\mathcal{B}) + \frac{k^2}{2}(\mathcal{A}^2 + \mathcal{AB} + \mathcal{BA} + \mathcal{B}^2) + O(k^3)\right).\end{aligned} \tag{3.74}$$

A comparison of $\xi(x,k)$ and $\xi^*(x,k)$ shows that the $O(k^2)$ are captured correctly and hence, this method is second order accurate.

3.8 Spectral Analysis

A numerical solution of the forced equatorial barotropic vorticity equation will, in general, be a superposition of waves of various frequencies and wavenumbers. In order to analyze the individual wave solutions, we use Fourier analysis to transform the solution into frequency-wavenumber domain, which permits a decomposition into individual components. The primary propagation direction of interest is the zonal (x) direction. Hence, we may simplify matters by studying the meridionally averaged zonal velocity $\langle u(x,t)\rangle$ given by

$$\langle u(x,t)\rangle = \frac{1}{2Y}\int_{-Y}^{Y} u(x,y,t)dy, \tag{3.75}$$

whose discrete analogue at each time step is

$$\langle u_j \rangle = \frac{1}{p} \sum_{k=1}^{p} u_{j,k} \quad , \tag{3.76}$$

where p is the number of grid points in the meridional direction. At each time step, we compute and store $\psi_{j,k}$ at a representative number K of evenly spaced strips in y. We also compute and store $\langle u \rangle$ at each time step. After the final time step, we may reassemble $\langle u(x,t) \rangle$ and view its contour plot, known as a Hovmoller diagram. (Here, It is advantageous to remove both the mean and the first few days of data, which correspond to the transient period and to make the function period in both space and time.) This will show the large scale structure of the zonal velocity field as it changes in time and allows us to see some wave structure. For a more detailed view of the wave structure, we must first perform a two-dimensional discrete Fourier transform on $\langle u \rangle$

$$\tilde{u}_{l,m} = \sum_{j=0}^{n-1} \sum_{k=0}^{T-1} \langle u_{j,k} \rangle e^{-2\pi i j l/n} e^{-2\pi i k m/K}, \tag{3.77}$$

where T is the number of time steps. Now $\tilde{u}$ is a function of wavenumber k and frequency ω. A contour plot of the power $\mathcal{P}(\tilde{u})$, where

$$\mathcal{P}(\tilde{u}_{l,m}) = \sum_{l=0}^{n-1} \sum_{m=0}^{T-1} |\tilde{u}_{l,m}|^2, \tag{3.78}$$

will show spectral peaks of distinct waves. Each wave may be isolated from the rest of the flow and its spatial structure (both zonal and meridional) and time evolution may be studied by the following process. First the region of interest in (k, ω) space is identified, *e.g.* $(k^* \pm \delta k, \omega^* \pm \delta\omega)$. Next, a two-dimensional (in x and t) discrete Fourier transform of the streamfunction ψ is performed for each of the K constant strips in y. These transformed streamfunctions may then be reassembled to form $\tilde{\psi}_{j,k,l}$, a three-dimensional streamfunction in (k, ω, y) space. The complement of the region of interest is masked out by setting everything in the domain outside of $(k^* \pm \delta k, \omega^* \pm \delta\omega)$ to zero. Then the inverse Fourier

transform is applied to the streamfunction, thereby yielding a function $\psi^*(x, y, t)$ which consists only of the wave structure corresponding to the spectral peak of interest.

Chapter 4

Validation

Numerical solution of the equatorial barotropic vorticity equation (EBVE) using the Arakawa Jacobian is validated by using a known solution. Comparisons are made with the exact solution and with the central scheme (which uses the conservative formulation of the EBVE), which was coded and validated in [8]. The planetary wave packets given by

$$\overline{\psi}(x, y) = \alpha \cos(k_1 x - \omega t) \sin(k_2 y) \tag{4.1}$$

are used for validation, where α tunes the strength of the wave packet, k_1 is the zonal wavenumber, k_2 is the meridional wavenumber, and $\omega = -k_1/(k_1^2+k_2^2)$ is the dispersion relation. These wave packets are defined on a periodic channel of zonal length $L = 40,000$ km and meridional width of $2Y = 10,000$ km and they solve the EBVE exactly. It can be easily seen that these wave packets have vanishing meridional velocity $\overline{v}$ at the channel walls ($y = \pm Y$) provided k_2 is chosen to be a multiple of π/Y. We set $k_1 = 8\pi/L$ and $k_2 = \pi/Y$, which we may abbreviate by writing $k_1 \equiv 4$ and $k_2 \equiv 1$ (corresponding to the fourth and first wavenumbers,

respectively). We fix the initial magnitude of the wind such that

$$\max_{x,y} \sqrt{\overline{u}(x,y,0)^2 + \overline{v}(x,y,0)^2} = 5m/s \tag{4.2}$$

and we run the code forward in time. A second order Runge-Kutta method is used, where Euler's method is used to make the initial prediction at each time step. This is an explicit method, where we use only information at time step n to calculate time step $n+1$. (Euler's method is essentially a first order truncation of the Taylor series of the time derivative, while a second order Runge-Kutta method represents a truncation after two terms of the Taylor series expansion of the time derivative.) A CFL condition with Courant number 0.8 is used to calculate the time step, i.e. for time step Δt, grid spacing Δx and Δy, and velocities $(\overline{u}, \overline{v})$, we choose $\Delta t = 0.8(\min(\Delta x, \Delta y)/\max(\overline{u}, \overline{v}))$. (This ensures that the time step is less than the time it takes the wave packet to propagate to adjacent cells.) Homogeneous Dirichlet boundary conditions at the wall are used.

Grid	5 days	10 days	15 days	20 days
128x75	1.281E-02	2.315E-02	3.255E-02	4.443E-02
256x150	7.275E-03	1.332E-02	1.899E-02	2.588E-02

Table 4.1: L1-norm relative error between exact solution for ξ and the numerical solution using the Arakawa Jacobian.

Grid	5 days	10 days	15 days	20 days
128x75	1.225E-02	2.224E-02	2.967E-02	4.002E-02
256x150	7.025E-03	1.286E-02	1.721E-02	2.330E-02

Table 4.2: L1-norm relative error between exact solution for ξ and the numerical solution using the central scheme.

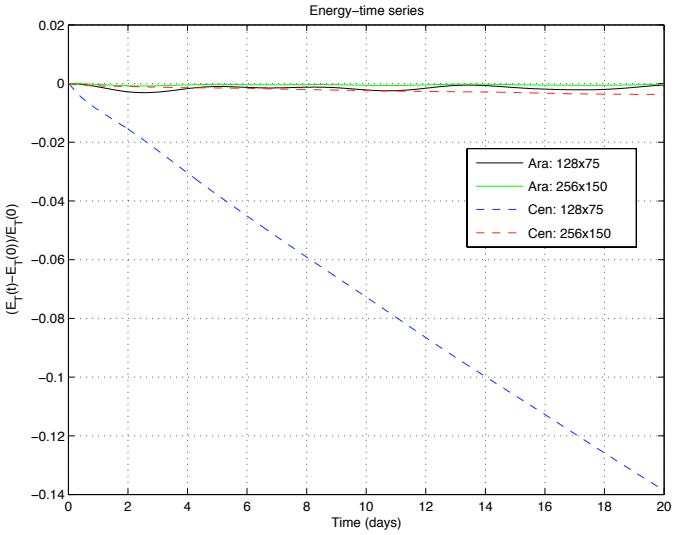

Figure 4.1: Energy-time plots using 128 x 75 and 256 x 150 grid points using the Arakawa method and the central scheme.

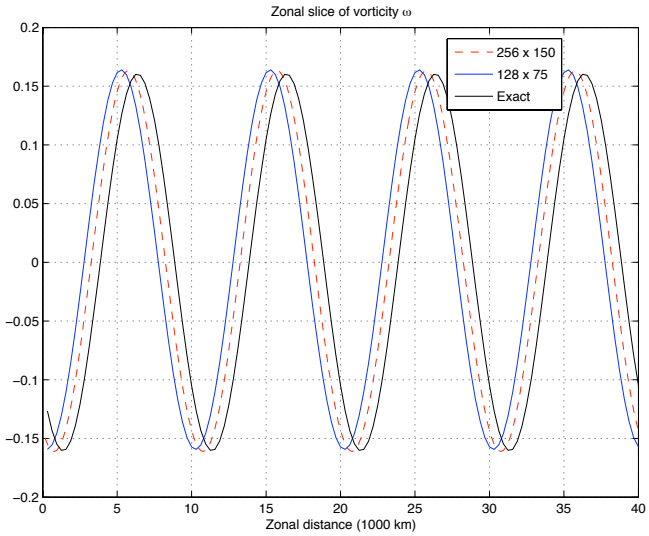

Figure 4.2: Zonal slice plot for the Arakawa method at $t = 20$ days of the vorticity ω at $y \approx 1600$ km.

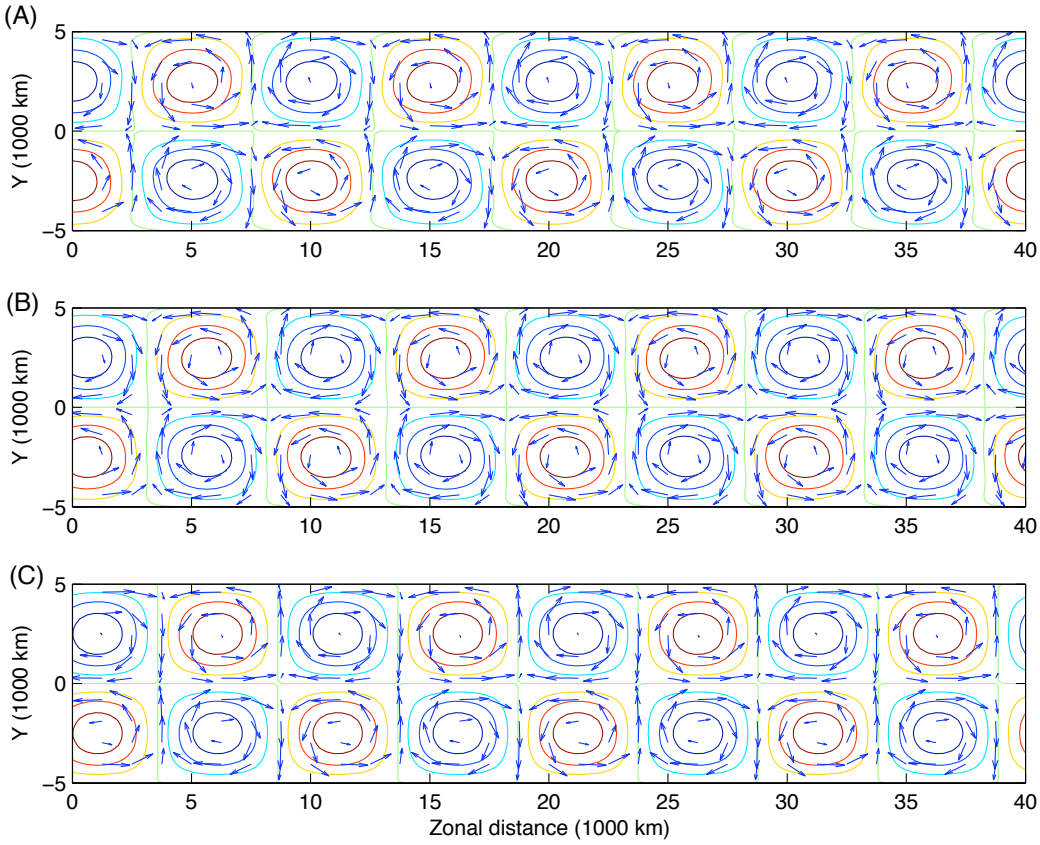

Figure 4.3: Two-dimensional structure of flow for Rossby wave packet after 20 days. Contour of the vorticity and velocity profile (arrows) for A) 128 x 75 grid points, B) 256 x 150, and C) exact solution.

In Table 4.1, we compute the L1-norm relative error, with respect to the potential vorticity ξ, between the exact and numerical solutions for two different grids, 128 x 75 and 256 x 150, at four consecutive times, 5, 10, 15, and 20 days, using the Arakawa Jacobian method. The same relative errors computed using the non-oscillatory central scheme are shown in Table 4.2.

An examination of the rate of convergence, found by taking the ratio of errors of the two grids at a given time, suggests that both methods are able to capture the large scale dispersive wave with an overall first order accuracy. Here, one would expect doubling of the spatial resolution to result in a quadrupling of the accuracy (since the methods used are second order accurate). That this is not seen is likely due to the boundary conditions, which are not exact (as suggested in [8]). Also, this method suffers from a phase error, as reported for the Central scheme [8].

Energy-time series plots in Figure 4.1 show that energy remains relatively constant in time for the Arakawa method, regardless of the number of grid points. (One would expect the energy to be exactly zero, to machine accuracy, with the Arakawa method. That this is not observed is thought to be due to the choice of boundary conditions. With exact boundary conditions, one would expect a different result.) The same is not true of the central incompressible scheme.

In Figure 4.2, a zonal slice of the vorticity $\omega = \xi - y$ at $y \approx 1600$ km and $t = 20$ days is shown for the grids 128 x 75 and 256 x 150 and is compared with the exact solution. From this plot, it is apparent that the Arakawa method slightly overestimates the phase speed of the Rossby wave packets since the exact solution is behind the westward travelling numerical solutions.

In Figure 4.3, contour plots of the vorticity ω are shown for the different grids

and the exact solution at $t = 20$ days . Velocity profiles are also superimposed. It appears that the structure and velocity field of the wave packet is nearly identical in all three cases, except that the numerical solution again appear to be travelling faster than the exact solution.

The y-plots of the L1-norm errors (after time $t = 5$ days) in the x-direction for the two grids are shown for both methods in Figures 4.4 and 4.5. It is interesting to note that while the central incompressible scheme has an error accumulation at the walls, the Arakawa method does not. This is most likely due to the fact that at each time step, the Arakawa Jacobian must vanish at the boundary $y = \pm Y$.

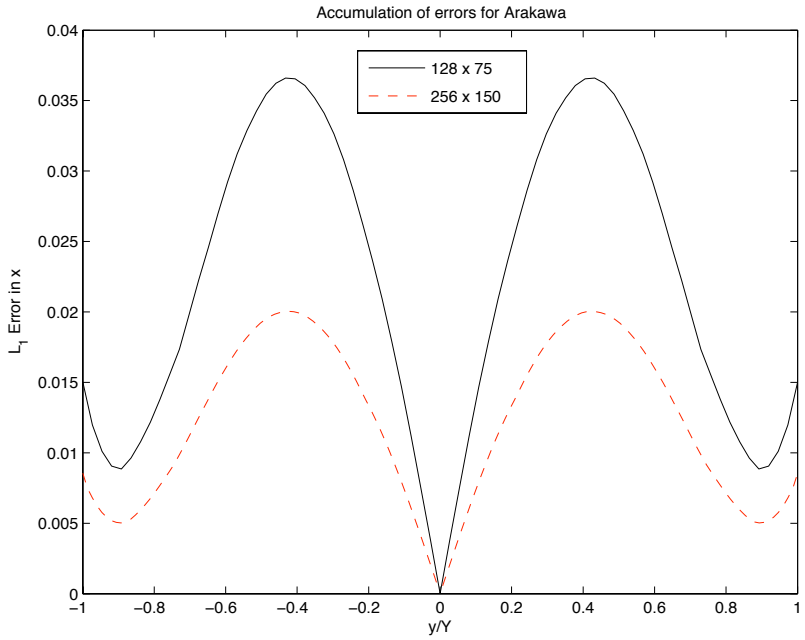

Figure 4.4: L1-norm error in x-direction versus y after $t = 5$ days for Arakawa method.

This is somewhat surprising, since both methods use second order schemes in both space and time. The same result was found in [8] and is thought to be the result of the choice of boundary conditions.

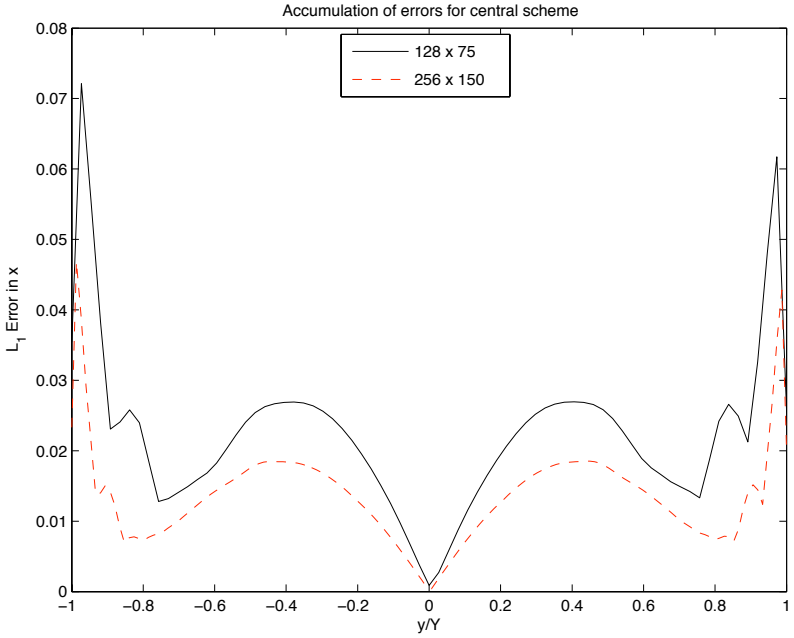

Figure 4.5: L1-norm error in x-direction versus y after $t = 5$ days for central scheme.

Chapter 5

Application: Barotropic response to a Kelvin wave forcing

5.1 Introduction

We will now apply the numerical methods of Chapter 3 to the model developed in Chapter 2. This will allow us to study the nonlinear interaction between the barotropic and the first baroclinic modes. In particular, we wish to consider the barotropic response to a baroclinic Kelvin wave forcing. We are careful to choose physically realistic parameters for the Kelvin wave forcing, based on observed equatorial Kelvin waves, since physically meaningful responses to such a forcing may provide insight into planetary wave dynamics and the teleconnection patterns between tropical and extra-tropical waves.

5.2 Numerical Results

We use the potential vorticity-streamfunction formulation of the forced equatorial barotropic vorticity equation, given by

$$\frac{\partial \overline{\xi}}{\partial t} + J(\overline{\psi}, \overline{\xi}) = f(x, y, t)$$

$$\triangle \overline{\psi} = \overline{\xi} - y \tag{5.1}$$

$$\overline{u} = -\frac{\partial \overline{\psi}}{\partial y}, \qquad \overline{v} = \frac{\partial \overline{\psi}}{\partial x} \tag{5.2}$$

$$f(x, y, t) = -\frac{1}{2}\left(\nabla \times [(\mathbf{v} \cdot \nabla \mathbf{v} + \mathbf{v} \nabla \cdot \mathbf{v})\ \hat{\mathbf{k}}]\right), \tag{5.3}$$

where an overbar represents a barotropic (*i.e.* vertically averaged or z-independent) component and $\hat{\mathbf{k}}$ represents the upward normal unit vector. Using this above equations, we choose a baroclinic Kelvin wave forcing whose projection onto the barotropic mode is

$$\mathbf{v} = (u, v), \quad u = \alpha \cos\left(k_0(x - ct)\right) e^{-y^2/2}, \quad v = 0. \tag{5.4}$$

This corresponds to a forcing function given by:

$$f(x, y, t) = \frac{k_0 y \alpha^2}{2} \sin\left(2k_0(x - ct)\right) e^{-y^2}. \tag{5.5}$$

In what follows, we shall omit the overbar since it is clear that all variables are now barotropic. We set $c = 5$ m/s, $k_0 \equiv 1$, and choose α such that, after applying the scaling due to nondimensionalization, $\alpha = \mathbf{v}_{max} = 10$ m/s. We choose these values to correspond reasonably closely to the characteristics of observed convectively coupled equatorial waves and the Madden-Julian Oscillation (MJO), where a phase speed of 5-10 m/s is observed for the MJO and a phase speed of roughly 15 m/s is observed for Kelvin waves [21]. The MJO has observed zonal wavenumbers of $k \equiv 1, 2$ and Kelvin waves are observed to have zonal wavenumbers of $k \equiv 4, 6$. The structure of the MJO resembles quite well that of a Kelvin wave with Rossby

gyres in its wake. Observed wind speeds for these waves are roughly 5-10 m/s.

The equations were solved on a periodic (in x) channel of zonal length 40,000 km and meridional length $\pm$ 5,000 km. The Jacobian formulation of the system was solved numerically at each time step using a second order Arakawa Jacobian [1] on a 256 x 150 grid. The initial condition $\psi(x, y, t = 0) = 0$, corresponding to a state of rest, was chosen. The time integration was performed using a second order Runge-Kutta method, with time steps chosen using a CFL condition, with Courant number = 0.8 [6]. (The CFL condition ensures a time step is chosen that is less than the time it takes for waves to travel to adjacent grid points. For time step Δt, grid spacing Δx and Δy, and velocities (u, v), we choose $\Delta t = 0.8(\min(\Delta x, \Delta y)/\max(u, v))$.) Each time step corresponded to 0.207 days, or roughly 5 hours. A total time integration of 102 days was used - with the first two days being removed during spectral analysis (as this corresponds to a transient period before statistical steady state).

A Hovmoller diagram, an energy time series, and a spectral plot are found below. The Hovmoller diagram is a diagnostic tool used in the atmospheric sciences community to show the zonal propagation of waves by taking the meridionally averaged zonal velocity and plotting contours of its time series.) We also show snapshots of the streamfunction of the total flow for one approximate period in the oscillating energy time series (approximate in the sense that the time series is not exactly periodic). In addition, the three distinct waves shown in the spectral plot were filtered and a snapshot (at a time corresponding to a local maximum in energy) of their streamfunctions was plotted. We also show the sum of the streamfunctions ψ_{waves} of the filtered waves, as well as the absolute value of the difference between ψ_{waves} and ψ_{tot}.

For comparison, we also show three other cases, each with $k_0 \equiv 2$, but with phase speeds $c = 5$ m/s, $c = 10$ m/s, and $c = 15$ m/s (with all other parameters the same).

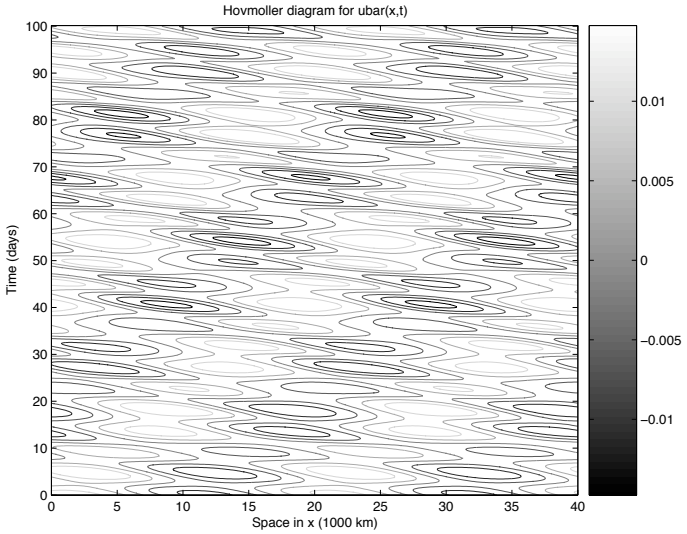

Figure 5.1: Hovmoller diagram for $k_0 \equiv 1$ and $c = 5ms^{-1}$

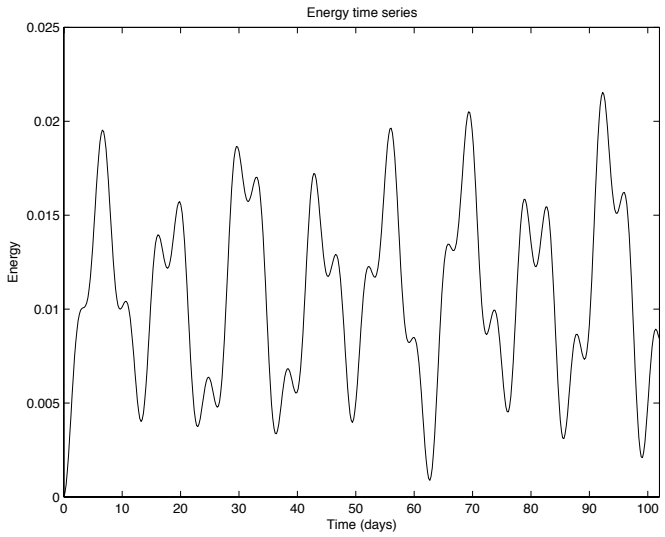

Figure 5.2: Energy timeseries for $k_0 \equiv 1$ and $c = 5ms^{-1}$

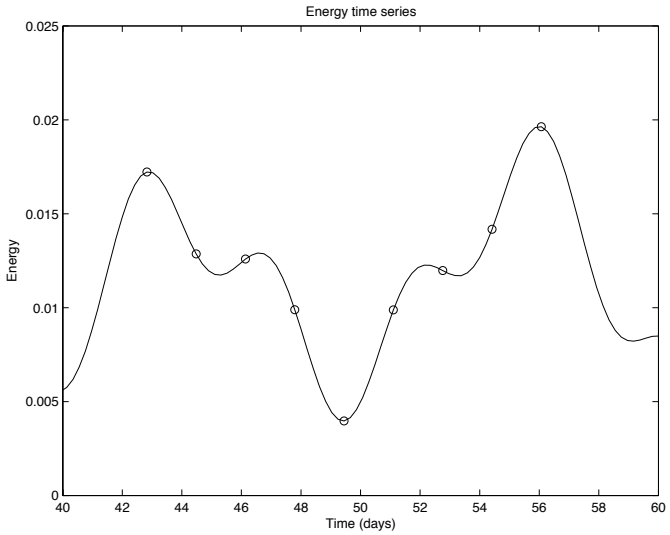

Figure 5.3: One approximate period in the energy timeseries for $k_0 \equiv 1$ and $c = 5ms^{-1}$

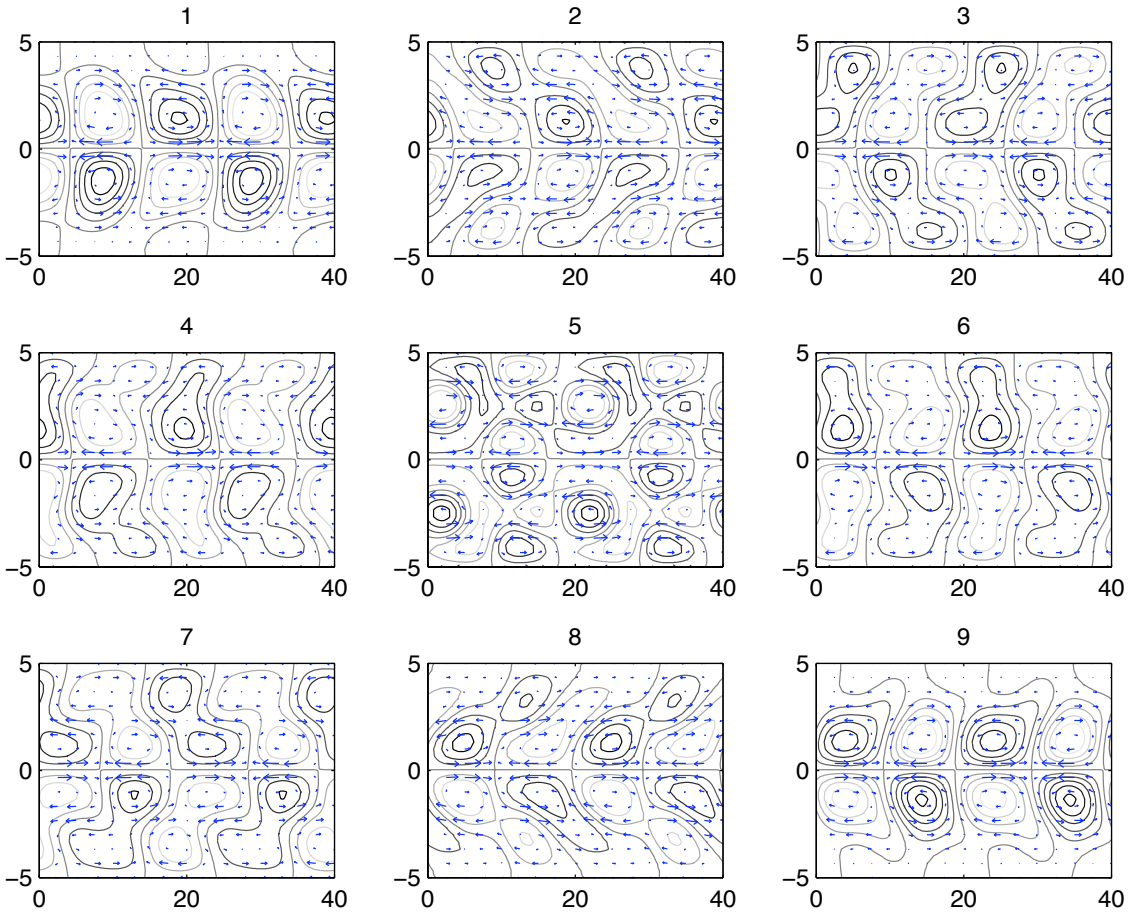

Figure 5.4: Streamfunction ψ during one energy period

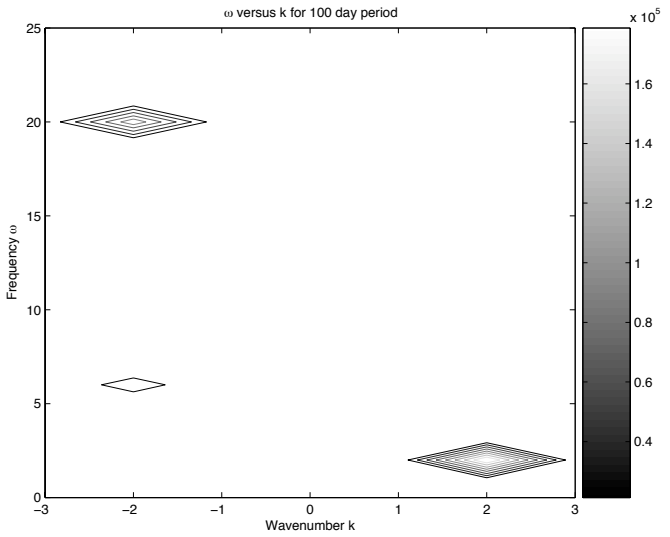

Figure 5.5: Spectral plot for $k_0 \equiv 1$ and $c = 5ms^{-1}$

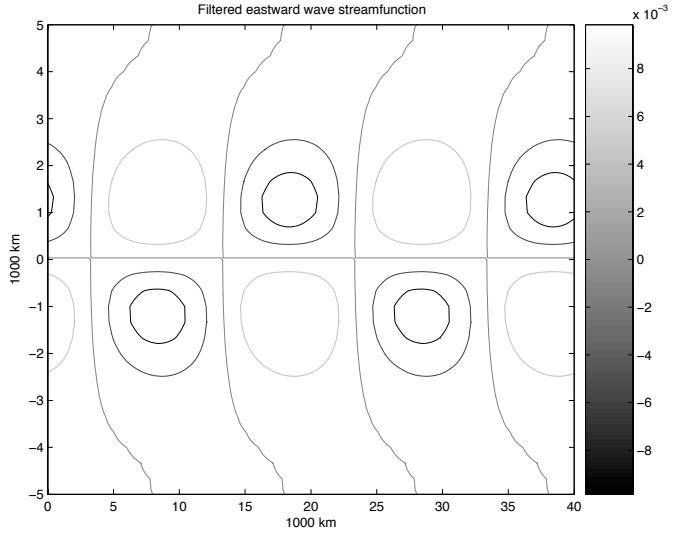

Figure 5.6: Snapshot of streamfunction for eastward propagating filtered wave with $k_0 \equiv 1$ and $c = 5ms^{-1}$

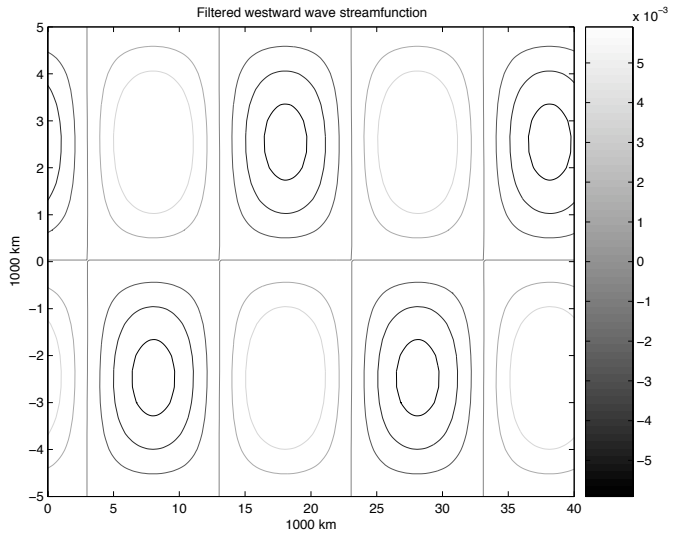

Figure 5.7: Snapshot of streamfunction for ($l \equiv 1$ Rossby) westward propagating filtered wave with $k_0 \equiv 1$ and $c = 5ms^{-1}$

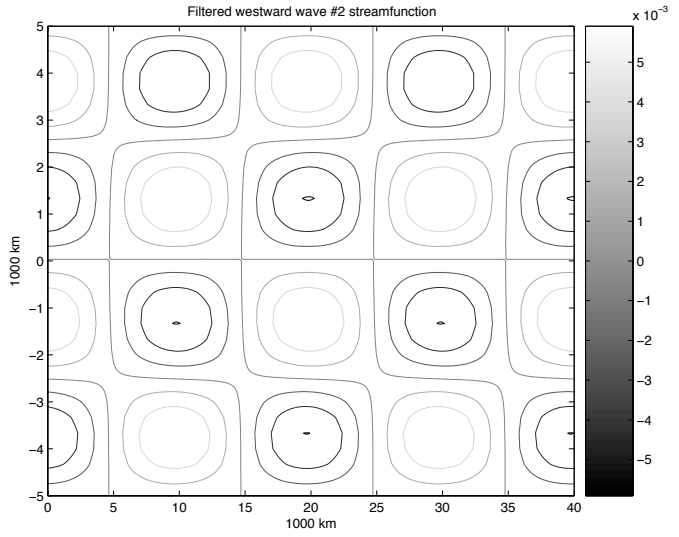

Figure 5.8: Snapshot of streamfunction for ($l \equiv 2$ Rossby) westward propagating filtered wave with $k_0 \equiv 1$ and $c = 5ms^{-1}$

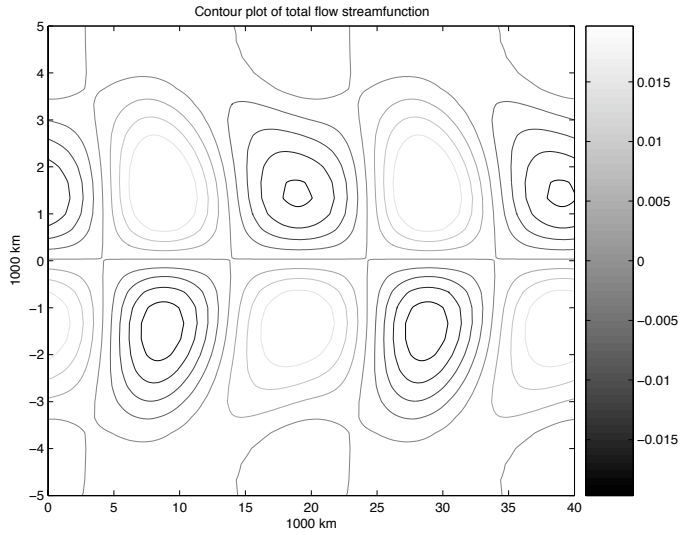

Figure 5.9: Snapshot of total flow streamfunction with $k_0 \equiv 1$ and $c = 5ms^{-1}$

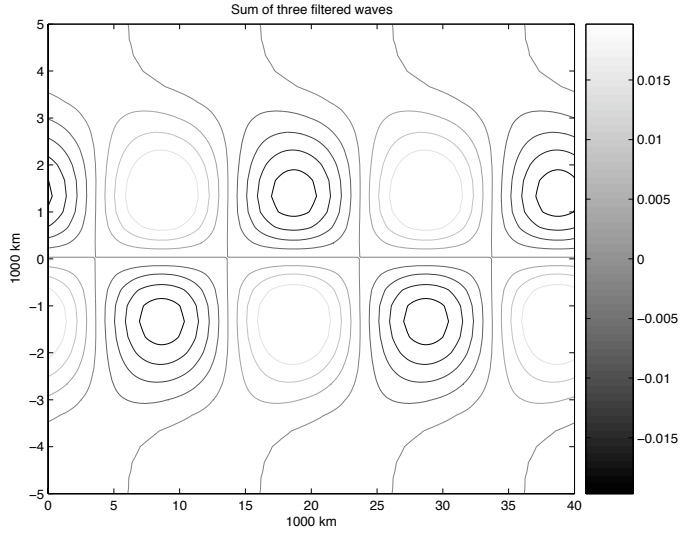

Figure 5.10: Snapshot of streamfunction for sum of three filtered waves with $k_0 \equiv 1$ and $c = 5ms^{-1}$

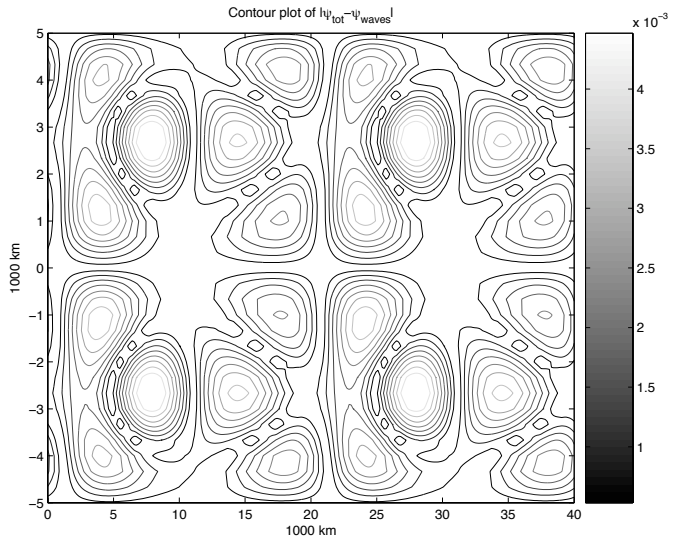

Figure 5.11: Snapshot of absolute value of difference between total flow and sum of three filtered waves

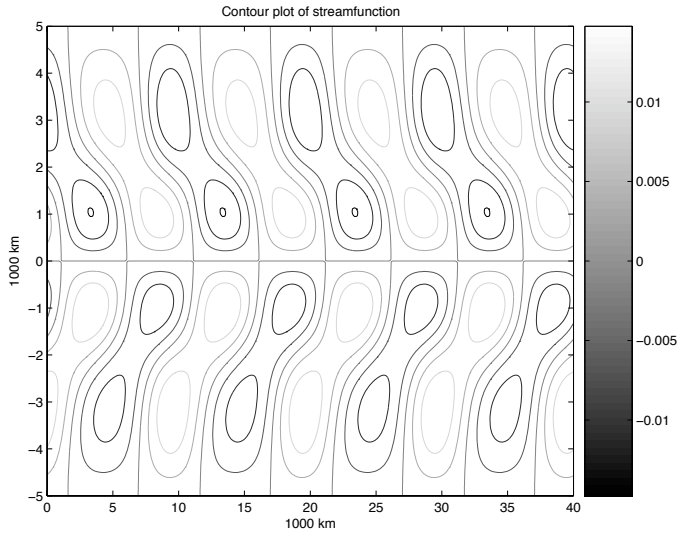

Figure 5.12: Total streamfunction for $k_0 \equiv 2$ and $c = 5ms^{-1}$

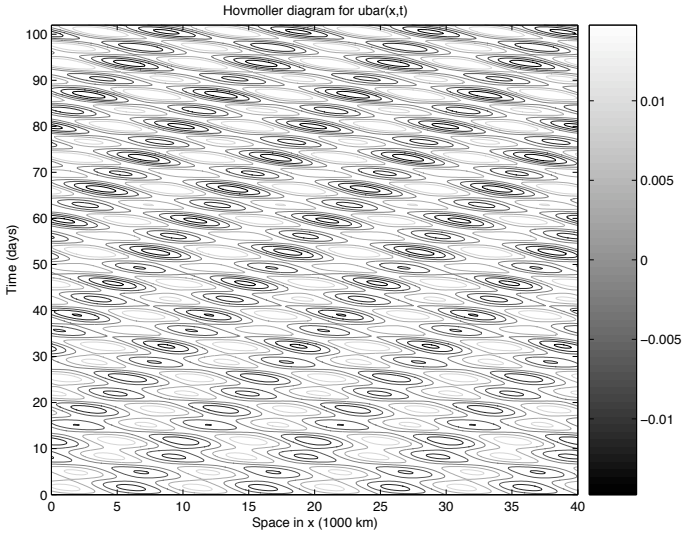

Figure 5.13: Hovmoller diagram for $k_0 \equiv 2$ and $c = 5ms^{-1}$

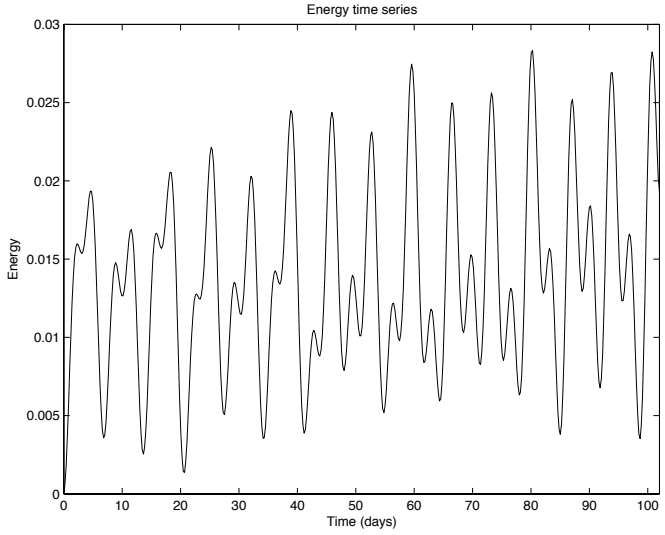

Figure 5.14: Energy Timeseries for $k_0 \equiv 2$ and $c = 5ms^{-1}$

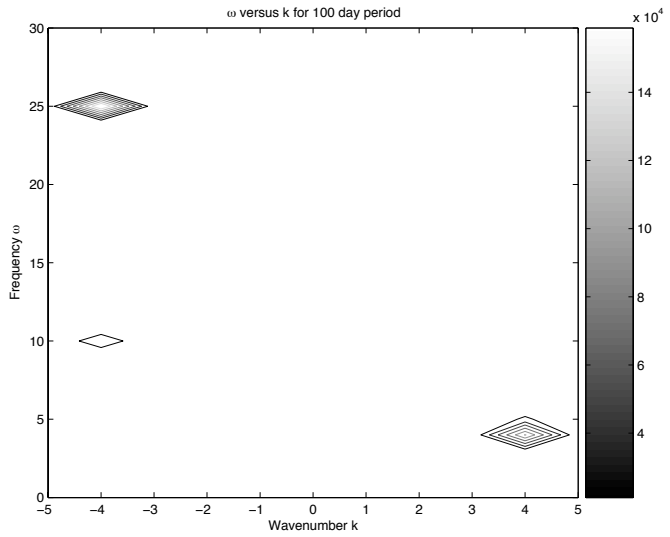

Figure 5.15: Spectral plot for $k_0 \equiv 2$ and $c = 5ms^{-1}$

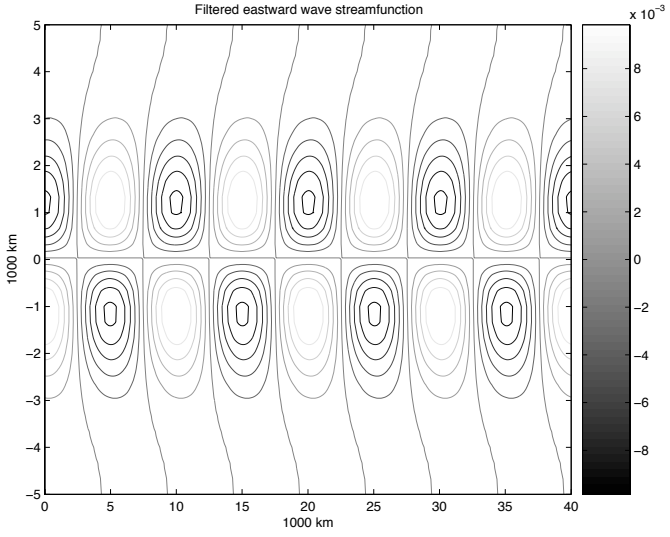

Figure 5.16: Snapshot of streamfunction for eastward propagating filtered wave with $k_0 \equiv 2$ and $c = 5ms^{-1}$

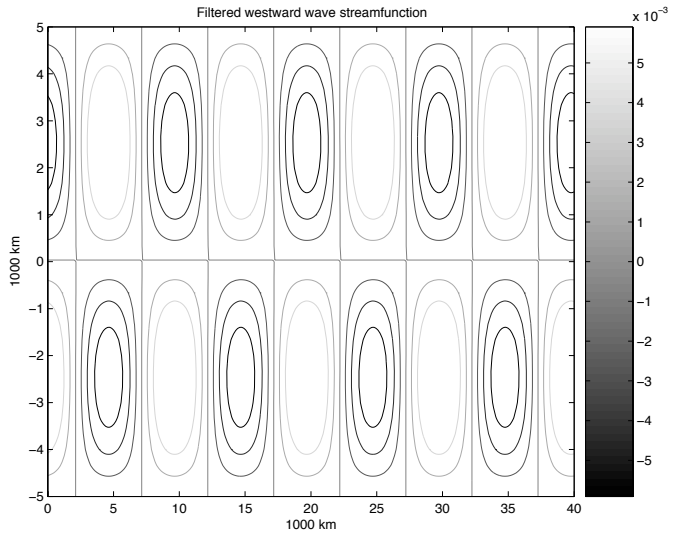

Figure 5.17: Snapshot of streamfunction for ($l \equiv 1$ Rossby) westward propagating filtered wave with $k_0 \equiv 2$ and $c = 5ms^{-1}$

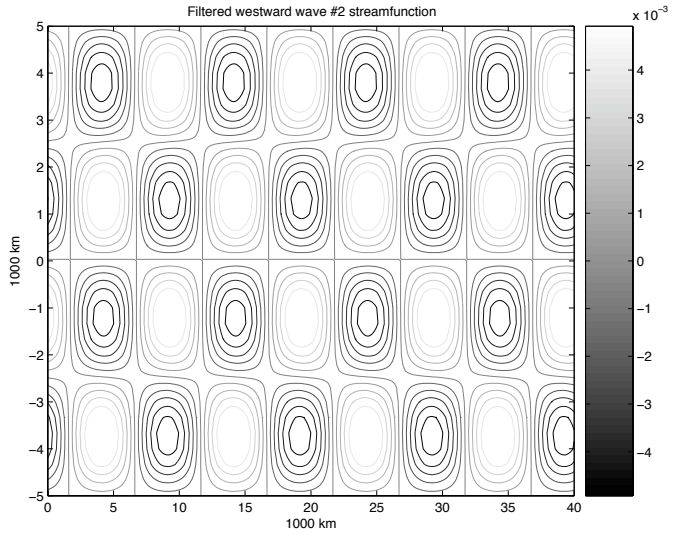

Figure 5.18: Snapshot of streamfunction for ($l \equiv 2$ Rossby) westward propagating filtered wave with $k_0 \equiv 2$

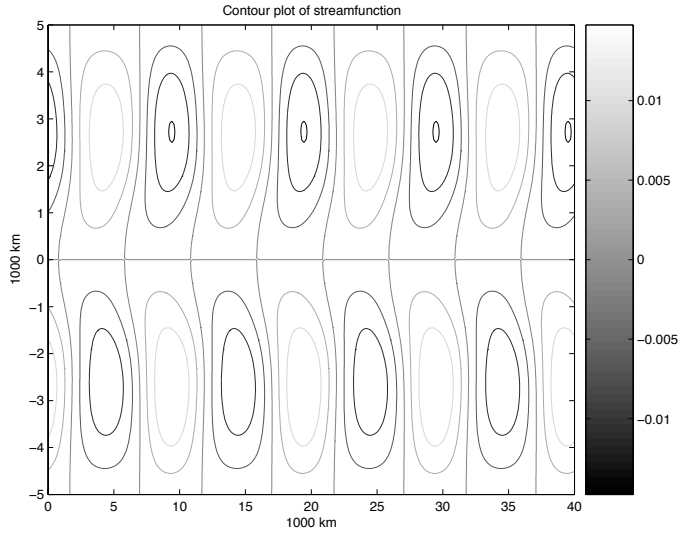

Figure 5.19: Total streamfunction for $k_0 \equiv 2$ and $c = 10ms^{-1}$

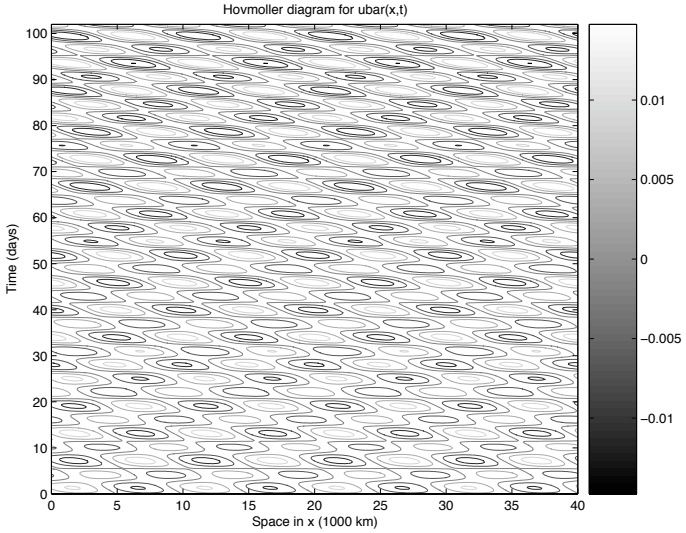

Figure 5.20: Hovmoller diagram for $k_0 \equiv 2$ and $c = 10ms^{-1}$

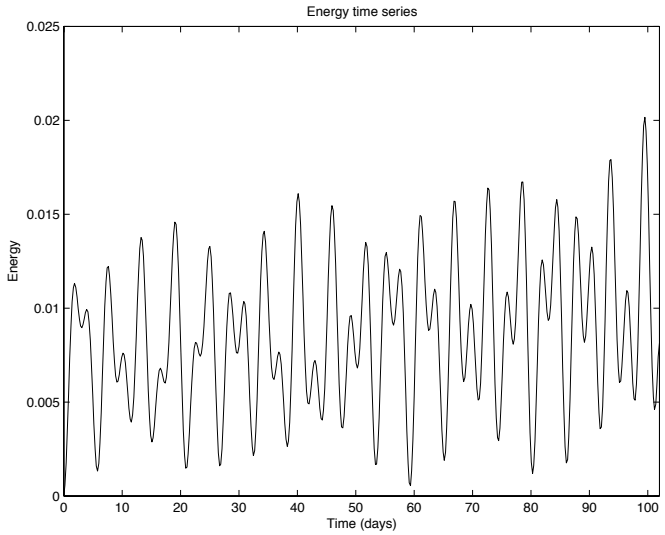

Figure 5.21: Energy Timeseries for $k_0 \equiv 2$ and $c = 10ms^{-1}$

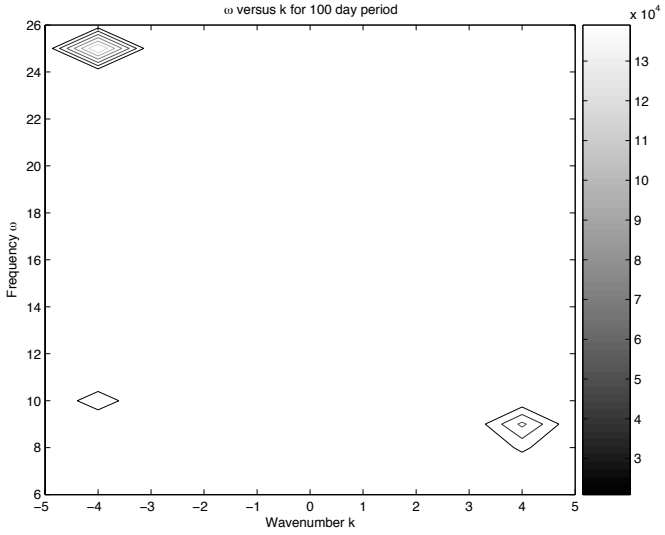

Figure 5.22: Spectral plot for $k_0 \equiv 2$ and $c = 10ms^{-1}$

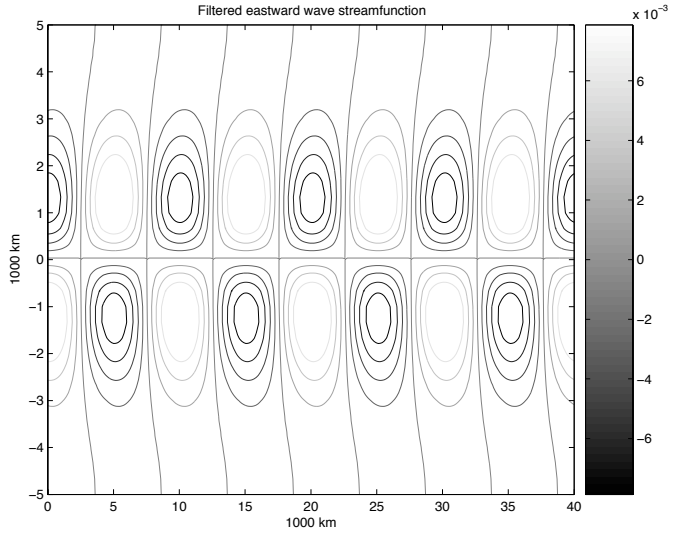

Figure 5.23: Snapshot of streamfunction for eastward propagating filtered wave with $k_0 \equiv 2$ and $c = 10ms^{-1}$

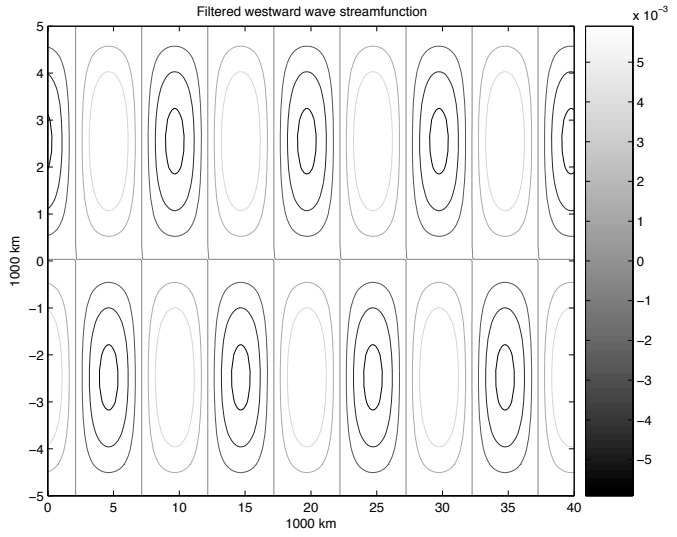

Figure 5.24: Snapshot of streamfunction for ($l \equiv 1$ Rossby) westward propagating filtered wave with $k_0 \equiv 2$ and $c = 10ms^{-1}$

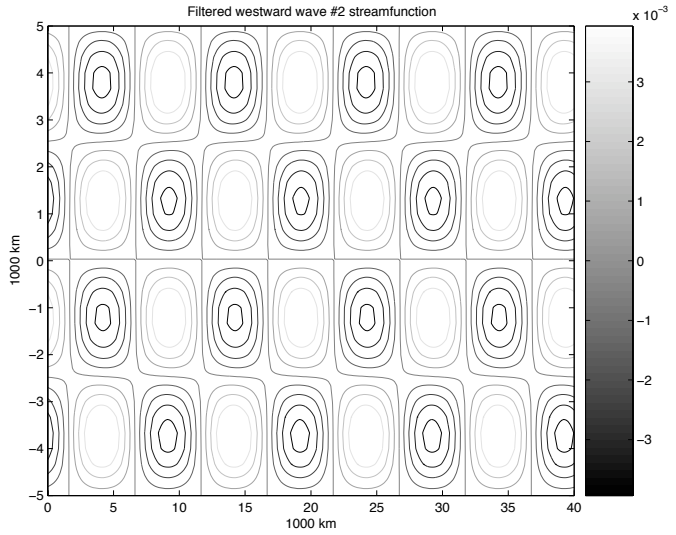

Figure 5.25: Snapshot of streamfunction for ($l \equiv 2$ Rossby) westward propagating filtered wave with $k_0 \equiv 2$ and $c = 10ms^{-1}$

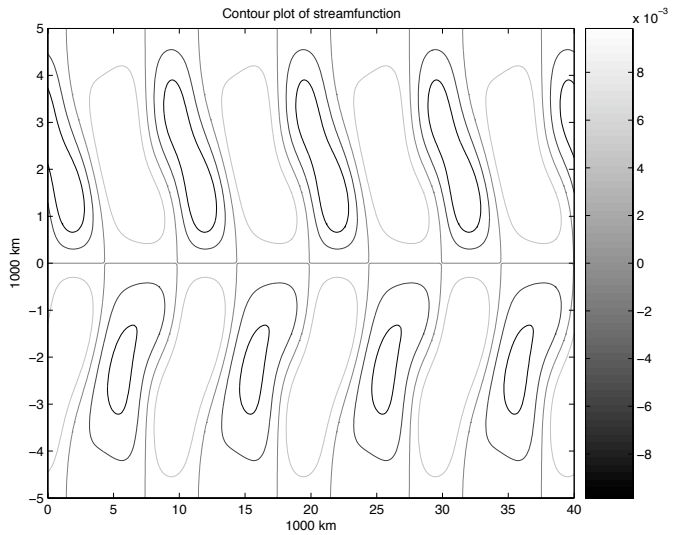

Figure 5.26: Total streamfunction for $k_0 \equiv 2$ and $c = 15ms^{-1}$

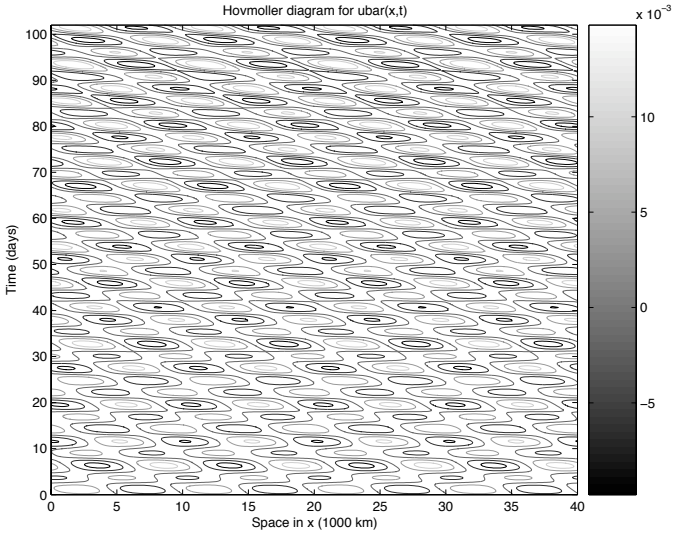

Figure 5.27: Hovmoller diagram for $k_0 \equiv 2$ and $c = 15ms^{-1}$

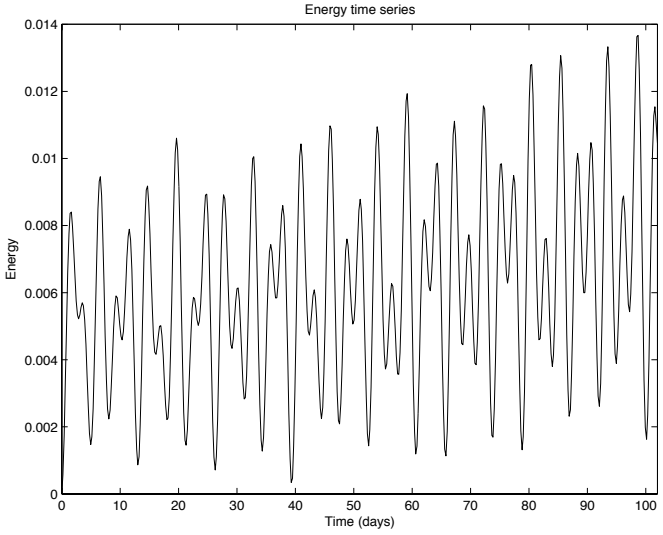

Figure 5.28: Energy Timeseries for $k_0 \equiv 2$ and $c = 15ms^{-1}$

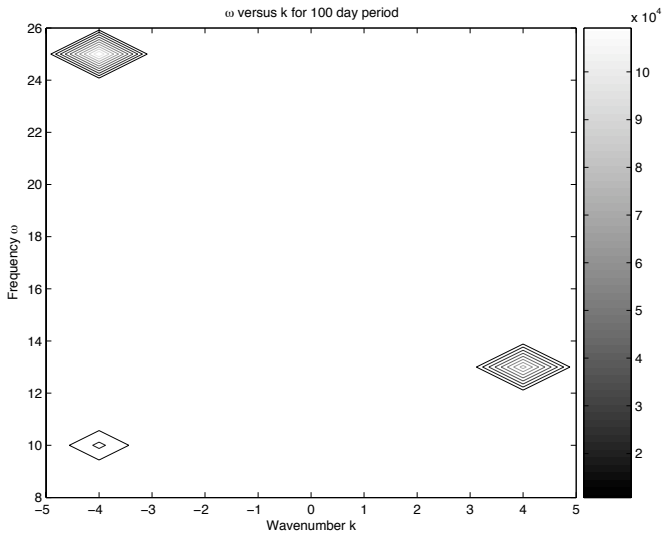

Figure 5.29: Spectral plot for $k_0 \equiv 2$ and $c = 15ms^{-1}$

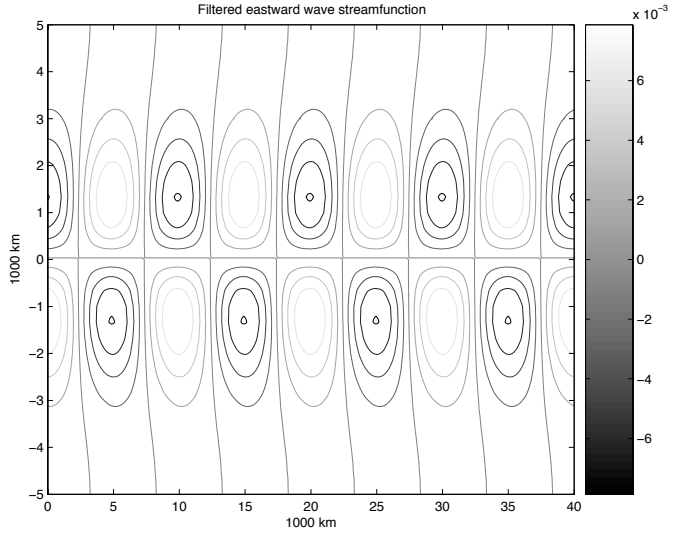

Figure 5.30: Snapshot of streamfunction for eastward propagating filtered wave with $k_0 \equiv 2$ and $c = 15ms^{-1}$

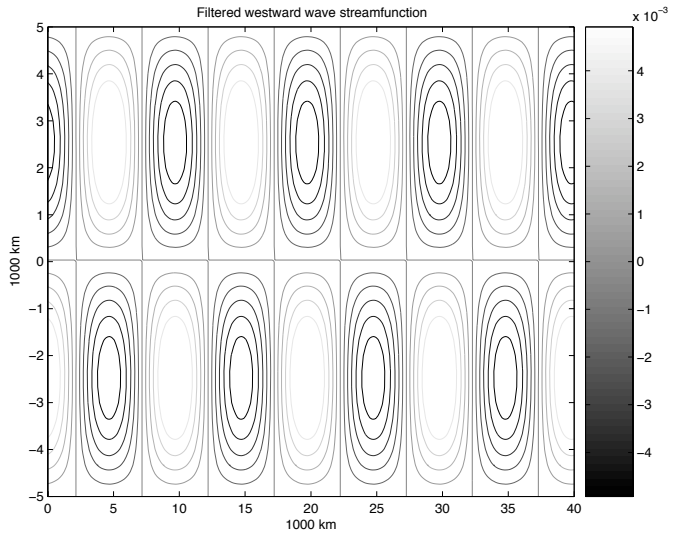

Figure 5.31: Snapshot of streamfunction for ($l \equiv 1$ Rossby) westward propagating filtered wave with $k_0 \equiv 2$ and $c = 15ms^{-1}$

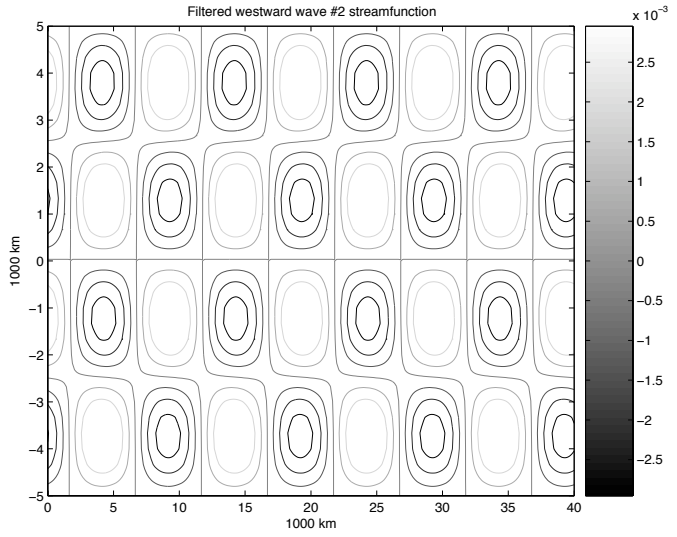

Figure 5.32: Snapshot of streamfunction for ($l \equiv 2$ Rossby) westward propagating filtered wave with $k_0 \equiv 2$ and $c = 15ms^{-1}$

We may make some initial observations about these results. The speed of each observed wave can be calculated using the frequency and wavenumber from the spectral diagram, using the relation $c_{num} = \omega/k$ and multiplying the the appropriate scaling factor, which depends not only on the nondimensionalization ($L \approx 1500$ km, $T \approx 8$ hours, $c \approx 50$ m/s). We note that in every case, the speed of the eastward travelling wave is in close agreement with the speed of the forcing. Thus, this eastward wave is phase-locked with the forcing, since both possess the same zonal wavenumber k. Similarly, the speed of the observed Rossby waves agree closely with their analytical values, which in nondimensional units is $c_{ana} = 1/(k^2 + l^2)$. The analytical and numerical speeds for each wave are shown below. Note that the speeds of observed waves depends only on choice of k_0, not on the phase speed c of the forcing function.

The fluctuations in the energy time series can be explained through constructive and destructive interference of the individual waves. In other words, when the individual waves have average zonal and meridional velocities that point in approximately the same direction, the total flow velocity will be large in magnitude, resulting in a local peak in energy. Conversely, when the individual waves have average zonal and meridional velocities that approximately interfere, the result will be a local minimum in the kinetic energy.

From the scale of the contour plots, we note that in each case the individual component waves are all of the same order of magnitude. There could be other numerical Rossby wave solutions but they do not compare in strength to the waves observed from the spectral plots. In fact, from the first case studied it is clear that the sum of the three filtered waves captures most of the total flow, as the residual term is an order of magnitude smaller than that of the individual waves. Only Rossby waves with the same zonal wavenumber as the eastward wave (and

the forcing) are observed. This curious fact will be discussed below.

Wave	c_{ana} (m/s)	c_{num} (m/s)
Eastward wave	5.00	4.63
Rossby ($l \equiv 1$)	45.05	46.30
Rossby ($l \equiv 2$)	13.24	13.89

Table 5.1: Analytical and numerical speeds of waves for $k_0 \equiv 1$

Wave	c_{ana} (m/s)	c_{num} (m/s)
Eastward wave	5.00	4.63
Rossby ($l \equiv 1$)	28.15	28.94
Rossby ($l \equiv 2$)	11.26	11.57

Table 5.2: Analytical and numerical speeds of waves for $k_0 \equiv 2$

5.3 Analysis of Results

We would like to understand why the Kelvin wave forcing excites only certain Rossby wave modes. In order to isolate the role of the streamfunction, we will rewrite the Jacobian term as $J(\psi, \xi) = J(\psi, \triangle\psi) + \psi_x$, where the subscript denotes partial differentiation. Our problem is defined for $x \in [0, L]$ and $y \in [-Y, Y]$ for the forced equatorial barotropic vorticity equation:

$$\frac{\partial}{\partial t}(\triangle\psi) + J(\psi, \triangle\psi) + \frac{\partial\psi}{\partial x} = F(x, y, t), \tag{5.6}$$

where $F(x, y, t) = C \sin(kx - \omega t))ye^{-y^2}$, $k = 2k_0$, $C = \alpha^2 k_0$, $\omega = ck_0$, $L = 40,000$ km, and $Y = 5,000$ km. We assume a solution $\psi(x, y, t)$ of the form

$$\psi = [A \cos(kx - \omega t) + B \sin(kx - \omega t)]g(y), \tag{5.7}$$

where $g(y)$ is an unknown function of y, A and B are constants, and we also assume, for the time being, that the Jacobian term $J(\psi, \triangle\psi)$ vanishes. Hence, our problem can be written as

$$\psi_{xxt} + \psi_{yyt} + \psi_x = C \sin(kx - \omega t))ye^{-y^2}, \tag{5.8}$$

Computing these partials gives the following

$$\psi_{xxt} = -g(y)k^2\omega[A \sin(kx - \omega t) - B \cos(kx - \omega t)], \tag{5.9}$$

$$\psi_{yyt} = g''(y)\omega[A \sin(kx - \omega t) - B \cos(kx - \omega t)], \tag{5.10}$$

$$\psi_x = -g(y)k[A \sin(kx - \omega t) - B \cos(kx - \omega t)]. \tag{5.11}$$

Substituting the partials into our original equation, we get

$$[g''(y) - \frac{(k^2\omega + k)}{\omega}g(y)][A \sin(kx - \omega t) - B \cos(kx - \omega t)] = \frac{C}{\omega} \sin(kx - \omega t))ye^{-y^2}. \tag{5.12}$$

This implies that $B = 0$, $A = C/\omega$, and that $g(y)$ is the solution to the differential equation

$$g''(y) - \lambda^2 g(y) = ye^{-y^2}, \quad \lambda^2 = \frac{(k^2\omega + k)}{\omega}. \tag{5.13}$$

Here the boundary conditions are given by $g(Y) = g(-Y) = 0$, which is implied from the condition that $v = \psi_x$ vanishes at $y = \pm Y$. The solution of this second order differential equation for $g(y)$ is

$$g(y) = A(e^{\lambda y} - e^{-\lambda y}) + \frac{\sqrt{\pi}}{8}\mathrm{erf}(-y + \lambda/2)e^{(\lambda^2 - 4\lambda y)/4} - \frac{\sqrt{\pi}}{8}\mathrm{erf}(y + \lambda/2)e^{(\lambda^2 + 4\lambda y)/4}, \tag{5.14}$$

where the constant A is given by

$$A = \frac{\sqrt{\pi}}{8}\frac{e^{\lambda^2/4}}{e^{2\lambda y} - 1}[\mathrm{erf}(-Y + \lambda/2)e^{-2\lambda Y} - \mathrm{erf}(Y + \lambda/2)] \tag{5.15}$$

A contour plot of the streamfunction of this solution for $k_0 \equiv 1$ and $c = 5\mathrm{m/s}$ is shown below and should be compared to the numerical result above. Return to

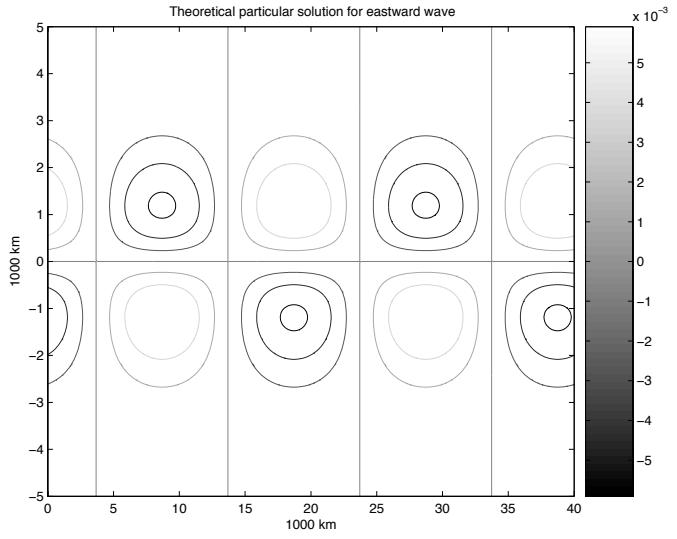

Figure 5.33: Theoretical streamfunction for particular solution with $k_0 \equiv 1$ and $c = 5ms^{-1}$

the original forced barotropic vorticity equation. It is clear that the homogeneous

(unforced) equation admits Rossby wave solutions of the form

$$\psi(x,y,t) = D\cos(k_n x - \omega_r t)\sin(l_m y), \quad k_n = \frac{2n\pi}{L}, \quad l_m = \frac{m\pi}{Y}, \tag{5.16}$$

where D is a constant, ω_r comes from the Rossby dispersion relation, and n and m are any positive integers. For each such solution ψ_i, it is also evident that

$$J(\psi_i, \triangle\psi_i) = 0. \tag{5.17}$$

Combining the above result with our assumption that for the Jacobian for the total flow vanishes implies that

$$J(\psi_0, \triangle\psi_0) = -\sum_{i\neq j} J(\psi_i, \triangle\psi_j), \quad i,j \in \{0,1,2,3,\dots\} \tag{5.18}$$

where ψ_0 represents the particular solution due to forcing and each ψ_i (for $i > 0$) represents a possible Rossby wave solution. Hence, the only permissible Rossby wave solutions are those which satisfy the above constraint.

It was remarked above that a forcing function $f(x,y,t)$ with zonal wave number k always generates an observed response consisting of waves of the same zonal wave number k. If we return to the particular solution found analytically above, we may express the meridional projection of this solution, $g(y)$, as a Fourier series. A plot of the power spectrum of the discrete Fourier transform of $g(y)$ is shown in Figure 5.34. Most of the power of $g(y)$ is contained in the first two modes $l \equiv 1$ and $l \equiv 2$. This is consistent with the observed Rossby wave response, which was always seen in the same two meridional modes. We note here that the spectral plots (for example, Figure 5.5) seem to imply that the $l \equiv 2$ mode is significantly weaker. This is not the case, as may be observed from snapshots of the filtered streamfunctions (see Figures 5.7 and 5.8). It is actually an artifact of the averaging process used in the spectral analysis, which results an underestimation of the spectral peaks of larger wavenumber waves. It seems plausible that a third, much

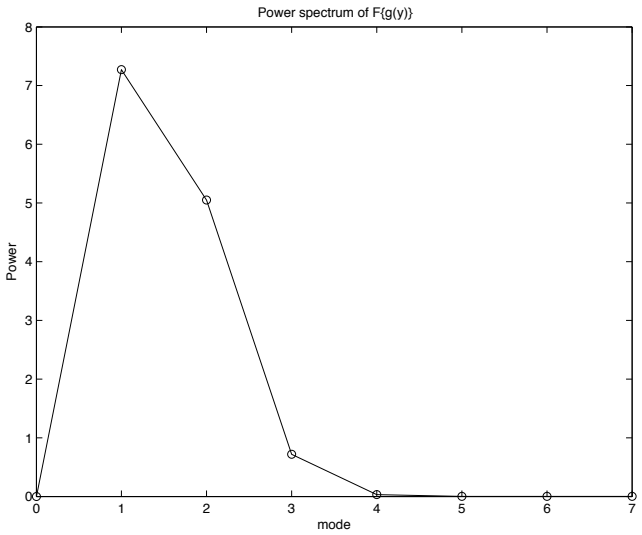

Figure 5.34: Power spectrum of $\mathcal{F}\{g(y)\}$

weaker, $l \equiv 3$ Rossby wave is also part of the response and that higher meridional wave number Rossby waves contribute only negligibly to the total flow. If this is true, a reasonable approximation of the eastward wave ψ_0 is

$$\psi_0 \simeq \cos(kx - \omega t)[a_1 \sin(l_1 y) + a_2 \sin(l_2 y) + a_3 \sin(l_3 y)], \tag{5.19}$$

where a_1, a_2, and a_3 can be found from the Fourier expansion of $g(y)$. This would provide a method of finding the approximate strengths D_j of the resulting Rossby waves in the response, given by expanding (5.19) and using $\psi_j = D_j \cos(kx - \omega_j t) \sin(l_j y)$ for $j \in 1, 2, 3$. In order to solve the resulting algebraic system, it may also be necessary to apply a suitable time averaging, thus eliminating any complications arising from the different frequencies of each interacting wave.

Chapter 6

Conclusion

The linear theory of equatorial waves is reviewed in detail, starting from the equatorial primitive equations. It is shown that the system decouples into an infinite number of shallow water equations, each governed by a z-dependent characteristic speed. Wave solutions resulting from this theory are highlighted. In particular, the barotropic Rossby wave solutions are highlighted, as they are of particular importance to tropical weather and climate. A Galerkin projection is applied to the linear evolution equation and a model involving a barotropic mode and a first baroclinic mode is developed. This model captures important nonlinear equatorial interactions. In particular, one may study the barotropic response of a baroclinic forcing of the equatorial barotropic voriticity equation by using a projection of the first baroclinic mode of the forcing on the barotropic system.

Numerical methods for the discretization of the forced equatorial barotropic vorticity equation are developed. First, finite differences are studied, then numerical methods for Poisson's equations are reviewed. Special attention is devoted to the properties of two-dimensional incompressible flow. This leads to a study of

Arakawa's method for discretizing the Jacobian of a two dimensional incompressible flow [1]. Methods of discretizing both time integration and forcing terms are also developed.

The numerical scheme for the free equatorial barotropic vorticity equations using the Arakawa Jacobian is validated using a known Rossby wave packet solution. A comparison is made with another numerical method (the central incompressible scheme [8]). It is shown that the Arakawa Jacobian method conserves energy nearly exactly and captures the dispersive wave structure of the test solution with an overall first order accuracy.

Solutions of the equatorial barotropic vorticity equation when forced by the barotropic projection of a baroclinic Kelvin wave are studied. It is shown that in every case studied, the response from the forcing consists of an eastward propagating phase-locked wave (representing the particular solution of the PDE corresponding to the forcing) and several westward travelling Rossby waves. The wavenumbers of the Rossby wave responses are highly constrained by the forcing. This is thought to be related to the spectral properties of the forcing. A method of predicting the strengths Rossby wave responses is proposed.

Bibliography

[1] A. Arakawa, *Computational design for long-term numerical integration of the equations of fluid motion: two-dimensional incompressible flow. Part I*, J. Comp. Phys. **1** (1966), 119-143.

[2] D. Durran, *Numerical methods for wave equations in geophysical fluid dynamics*, Springer-Verlag, New York, 1999.

[3] R. Fjørtoft, *On the changes in the spectral distribution of kinetic energy for twodimensional, nondivergent flow*, Tellus **5** (1953), 225-230.

[4] D.M.W. Frierson, A.J. Majda and O.M. Pauluis, *Large scale dynamics of precipitation fronts in the tropical atmosphere: a novel relaxation limit*, Comm. Math. Sci. **2** (2004), 591-626.

[5] A. Gill, *Atmosphere-ocean dynamics*, Academic Press, New York, 1982.

[6] G.H. Golub and J.M. Ortega, *Scientific computing and differential equations*, Academic Press, San Diego, 1992.

[7] R. Haberman, *Elementary and applied partial differential equations*, Prentice-Hall, Englewood Cliffs, 1983.

[8] B. Khouider, and A. Majda, *A non-oscillatory balanced scheme for an idealized tropical climate model. Part I: Algorithm and validation*, Theor. Comput. Fluid Dyn. **19** (2005), 331-354.

[9] B. Khouider, and A. Majda, *A nonoscillatory balanced scheme for an idealized tropical climate model. Part II: Nonlinear coupling and moisture effects*, Theor. Comput. Fluid Dyn. **19** (2005), 355-375.

[10] B. Khouider, and A. Majda, *Multicloud Convective Parametrizations with Crude Vertical Structure*, Theor. Comput. Fluid Dyn. **20** (2006), 351-375.

[11] B. Khouider, and A. Majda, *Model Multicloud Parametrizations for Convectively Coupled Waves: Detailed Nonlinear Wave Evolution,*, Dynam. Atmos. Oceans **42** (2006), 59-80.

[12] B. Khouider, and A. Majda, *A simple multicloud parametrization for convectively coupled tropical waves. Part I: Linear analysis*, J. Atmos. Sci. **63** (2006), 1308-1323.

[13] B. Khouider, and A. Majda, *A simple multicloud parametrization for convectively coupled tropical waves. Part II: Nonlinear simulations*, J. Atmos. Sci. **64** (2007), 381-400.

[14] D. Levy and E. Tadmor, *non-oscillatory central schemes for the incompressible 2-D Euler equations*, Mat. Res. Let. **4** (1997), 321-340.

[15] A. Majda, *Introduction to PDEs and waves for the atmosphere and ocean*, American Mathematical Society and New York University, Providence, 2003.

[16] A. Majda, and J. Biello, *The nonlinear interaction of barotropic and equatorial baroclinic Rossby waves*, J. Atmos. Sci. **60** (2003), 1809-1821.

[17] T. Matsuno, *Quasi-geostrophic motions in the equatorial area*, J. Met. Jap. **44** (1966), 25-41.

[18] J. Pedlosky, *Geophysical Fluid Dynamics*, 2nd ed., Springer-Verlag, New York, 1987.

[19] N.A. Phillips, *An example of non-linear computational instability*, The atmosphere and the sea in motion, Rossby memorial volume, 501-504. Rockefeller Institute Press, New York, 1959.

[20] W.H. Press, S.A. Teukolsky, W.T. Vetterling and B.P. Flannery *Numerical recipes in Fortran*, 2nd ed., Cambridge University Press, New York, 1992.

[21] M. Wheeler and G. Kiladis, *Convectively coupled equatorial waves: analysis of clouds and temperature in the wavenumber-frequency domain*, J. Atmos. Sci. **56** (1999), 374-399.